

**Radiative Transfer in lognormal
multifractal Clouds
and
Analysis of
Cloud liquid Water Data**

by
Gerd Brösamlen

A Thesis submitted to the Faculty of Graduate Studies and
Research in partial fulfillment of the requirements for the degree of
Master of Science

**Department of Physics
McGill University
Montréal, Québec
Canada**

March 1994

© Gerd Brösamlen 1994

(short title)

**Radiative Transfer in lognormal
multifractal Clouds**

by

Gerd Brösamlen

**A Thesis submitted to the Faculty of Graduate Studies and
Research in partial fulfillment of the requirements for the degree of
Master of Science**

**Department of Physics
McGill University
Montréal, Québec
Canada**

March 1994

© Gerd Brösamlen 1994

...meinen Eltern Heide und Walter gewidmet

Abstract

The study of radiative transfer in multifractal clouds is of great interest, an important application being to Global Climate Models. In this work we develop a formalism analogous to the multifractal singularity formalism for understanding photon scattering statistics in radiative transfer in multifractals, and test the results numerically on lognormal multifractals. Although the results are only exactly valid in the thick cloud limit, the approximation is found to be quite accurate down to optical thickness of $\tau \approx 1 - 10$, so the results may be widely applicable. Furthermore we show the possibility of "renormalizing" the multifractal by replacing it with a near equivalent homogeneous medium but with a "renormalized" optical thickness $\tau^{1/(1+C_1)}$ where C_1 is the codimension of the mean singularity of the cloud. We argue that this approximation is likely to continue to be valid for multiple scattering, and is also compatible with recent results for diffusion on multifractals. Finally we analyze cloud liquid water content data and estimate the universal multifractal indices. We find that the scaling is respected over the whole range 5m - 330km and that the cloud can in fact be reasonably described by a lognormal multifractal.

Résumé

L'étude des transferts radiatifs dans les nuages de type multifractal est d'un grand intérêt, particulièrement en vue de des conséquences pour les Modèles de Climat Globaux. Ce mémoire présente un formalisme analogue à celui des singularités multifractales afin de comprendre les statistiques de la rétro-diffusion des photons (transfert radiatif) dans un multifractal. Les prédictions sont comparées aux résultats numériques obtenus avec des multifractals log-normaux. Même si les résultats ne s'appliquent qu'aux nuages optiquement épais, l'approximation s'est révélée bonne pour des épaisseurs optiques de l'ordre de $\tau \approx 1-10$; ainsi ces résultats sont applicables assez généralement. De plus, nous montrons qu'il est possible de "renormaliser" le multifractal en le remplaçant par un milieu homogène presque équivalent mais ayant une épaisseur optique $\tau^{1/(1+C_1)}$ où C_1 est la co-dimension de la singularité moyenne du nuage. Nous prétendons que cette approximation devrait être valable pour la rétro-diffusion multiple et qu'elle est compatible avec les résultats récents de diffusion dans les multifractals. Finalement, nous analysons les données de quantité liquide d'eau des nuages et estimons les paramètres multifractals fondamentaux. Nous trouvons que l'invariance d'échelle est respectée pour une fourchette de 5m à 330km et que le nuage peut raisonnablement être décrit par un multifractal log-normal.

Table of Contents

Abstract	i
Résumé	ii
Table of Contents	iii
Acknowledgments	iv
Contributions to Original Knowledge	v
1. Introduction	1
1.1 Context	1
1.2 Outline	4
2. Basic Theory	6
2.1 Scaling and Fractal Dimension	6
2.2 Multifractal Clouds	7
2.3 Bare and Dressed Multifractals	12
2.4 The Equation of Radiative Transfer	13
2.5 Singularity Formulation of Scattering in Multifractal Clouds	16
3. Numerical Simulations and Dressed Statistics	20
3.1 Simulating the Multifractal Clouds	20
3.2 Simulating the Transport	20
3.3 The Probability Distribution Exponent	21
3.4 Limits of Validity for the Probability Distribution Exponent	25
a) Breakdown for low extinction coefficients	25
b) Limits on the Range of Photon Path Length Singularities	26
3.5 Moment Scaling Exponent	29
3.6 Limits of Validity for the Moment Scaling Exponent	32
4. Renormalization	33
4.1 Direct Transmission	33
4.2 Some Considerations on Multiple Scattering	36
4.3 Comparison with Diffusion	38
5. Analysis of empirical cloud data	40
5.1 The Cloud Liquid Water Data	40
5.2 Power spectrum	42
5.3 Structure function	46
5.4 Transformation of the Data into a Conserved Multifractal	49
5.5 Double Trace Moment Analysis	51
5.6 Analysis of the statistical moments	54
5.7 Analysis of the probability distribution exponent	56
5.8 Evidence for lognormal multifractal clouds	58
5.9 Conclusions of the empirical cloud data analysis	61
6. Conclusions	62
Appendix	64
A1 Evaluation of the Moment Scaling Exponent	64
A2 Laplace Method for the Evaluation of the Probability Distribution Exponent	66
Bibliography	67

Acknowledgments

I would like to express my deep gratitude to my supervisor Shaun Lovejoy* from the Department of Physics at McGill University. His scientific expertise and intuition were the nucleus of this project and his enthusiasm encouraged me to pursue this research energetically. He was very patient and encouraging, despite my occasional lack of motivation. Working together with him revealed the true meaning of the word cooperation.

My thankfulness is also addressed to Brian Watson at the Physics Department at St. Lawrence University in Canton, New York. He contributed to the radiative transfer part of this work which benefited me particularly in my initiation to this field. In addition his responds helped me to defeat the unavoidable periods of frustration

Many other scientists and students deserve my appreciative recognition for helpful discussions, exchange of knowledge, and support in the programming. This is especially the case for those who joined my research group at the time of my graduate studies. Nicolas Desaulniers-Soucy, Pablo Garrido, Daniel Harris, Charles Hooge, Chris Larnder, Daniel Lavallée**, Greg Lewis, Jean-François Maloun, Sean Pecknold, Daniel Schertzer***, François Schmitt***, and Patricia Silas. In particular I acknowledge Sean Pecknold, Charles Hooge and Chris Larnder for the provision of software.

I would like to thank Graham Cross for his encouragement during my graduate studies and the careful review of the manuscript.

Last but not least I want to voice my gratefulness to my family, my friends and acquaintances here in Canada as well as in other parts of the world for their direct or indirect support. Especially I want to thank my fiancée Liza Maria for her love, understanding and patience during this time.

* presently on Sabbatical at the Laboratoire de Météorologie Dynamique, Université P & M. Curie, 4 Place Jussieu, F-75252, Paris Cedex 05, France

**Earth-Space Research Group, Computer Systems Lab - Ellison Hall, University of California, Santa Barbara, CA 93106

***Laboratoire de Météorologie Dynamique, Université P & M. Curie, 4 Place Jussieu, F-75252, Paris Cedex 05, France

Contributions to Original Knowledge

This thesis is the first study on scattering statistics in lognormal multifractal media as well as the first complete estimation of the universal multifractal indices of cloud liquid water data

The "Numerical Simulations and Dressed Statistics" (chapter 3) is an original contribution by the author in order to justify the theory (section 2.5), "Singularity Formulation of Scattering in Lognormal Multifractals", obtained in cooperation with Shaun Lovejoy* , Brian Watson** and Daniel Schertzer*** which itself finds no comparable theory throughout literature. The "Renormalization" approach (chapter 4.) was developed in cooperation with the above and consist also of new ideas. The author is among the first to systematically investigate cloud liquid water data for the universal multifractal indices α and C_1 by the involved analysis techniques in chapter 5. All the figures are original.

* Department of Physics, McGill University, 3600 rue University, Montréal, Québec, H3A 2T8, Canada.

** Physics Department, St. Lawrence University, Canton, N Y. 13617.

*** Laboratoire de Météorologie Dynamique, Boîte 99, Université P&M Curie, 4 Place Jussieu, Paris F-75252, Cedex 05, France.

1. Introduction

1.1 Context

The problem of specifying the radiation field in an atmosphere which scatters light originated in Lord Rayleigh's investigations in 1871 on the illumination and polarization of the sunlit sky. But the fundamental equation of transfer governing Rayleigh's particular problem had to wait seventy-five years for their formulation and solution (Chandrasekhar 1946). The subject was given a fresh start under more tractable conditions, when in 1905 Arthur Schuster formulated a problem in radiative transfer in an attempt to explain the appearance of absorption and emission lines in stellar spectra (Schuster 1905). Since that time the subject of Radiative Transfer has been investigated principally by astrophysicists and geophysicists, though it also generated interest to the physics community (e.g. in the theory of the diffusion of neutrons).

The problem of determining radiative properties of inhomogeneous clouds is notoriously difficult and remains an active field of research. In fact, all problems that require a realistic account of the effect of radiation in a cloudy atmosphere must be concerned with the spatial (and temporal) variability of clouds and the impact of this variability on the radiative process of interest. Many applications readily come to mind, as for example global climate models which require the radiative budget of some volume of atmosphere. Most numerical models of the radiative effect of clouds on the Earth's climate have assumed plane-parallel geometry and thus entail significant errors. Other applications are remote sensing studies of clouds and precipitation.

The term "inhomogeneous clouds" is to be taken in a very broad sense. We include cloud fields as well as isolated internally homogeneous clouds of finite horizontal extent. In fact this field of research has become known as "multidimensional" * radiative transfer and exactly complements the well developed theory of plane-parallel media where radiation field and/or optical properties vary in the vertical only (See Lenoble 1977 for an extensive review). The upcoming discussion is restricted to the horizontally inhomogeneous atmosphere where we can distinguish three different approaches: the non-fractal, the fractal (monofractal), and the multifractal.

The study of fractals and multifractals is a relatively new field which in recent years has gained growing recognition and a mushrooming interest, particularly in physics and geophysics. Geophysical systems such as the atmosphere exhibit extreme variability

* in the following called "horizontally inhomogeneous" to avoid any possible confusion with the term "multiple (fractal) dimension"

over ranges of scale which can exceed factors of 10^9 . The dynamical models of these systems used for example in weather prediction, are typically scale invariant hence in principle can admit multifractal solutions. A growing body of theoretical and empirical work is showing that geophysical systems do indeed obey scaling symmetries over considerable ranges (for reviews, see Korvin 1992, see also papers in Scholz and Mandelbrot 1989, Schertzer and Lovejoy 1991, Lam and De Cola 1993). Thanks to advances in scaling ideas, particularly multifractals and generalized scale invariance, models can now be sufficiently realistic that they can be used for simulating various physical processes including transport phenomena.

Before we review some of the most important contributions to the radiative transfer problem in inhomogeneous, scale invariant media, a very concise summary of the non-fractal approaches is given here (for a more detailed overview see Lovejoy et al 1990 or Davis et al 1992). Although the distinction is somewhat arbitrary, non-fractal approaches can be divided into two categories:

In the first category, which is the most extensively studied in literature, clouds are internally homogeneous but non plane parallel boundary conditions impose horizontal gradients in the radiation field. Some researchers investigate simple geometrical shapes (e.g. cubes, cylinders, spheres) by various methods (e.g. Preisendorfer and Stephens 1984, Stephens and Preisendorfer 1984), others study the statistical mixture of these noninteracting cloud fields (e.g. Ronnholm et al. 1980, Welch and Zdunkowski 1981) and also do research on genuine cloud fields, modeled by one and two dimensional arrays of these entities (e.g. Wendling 1977, Titov 1980, Davies 1984).

The second category consists of models in which the internal optical depth field varies in at least one horizontal direction. To mention one of these physically more relevant contributions, Stephens 1988a,b offers a general formalism and discusses variability over many scales in connection with (two-dimensional) satellite imagery.

Starting with Gabriel et al 1986, fractal models of clouds have been used to numerically study the radiative properties of extremely variable clouds. These authors showed that even spatial variabilities confined to a range as small as a factor of 32 would in principle be sufficient to explain the apparent large discrepancies (factors of 10 are cited) between *in situ* and satellite estimates of cloud amount (the "albedo paradox"). Since then, fractal models have been used in a series of papers (Lovejoy et al 1988, 1990; Davis et al 1988, 1990; Gabriel et al 1990) who used simple fractal (" β ") models to investigate the "bulk" properties such as overall mean albedo and transmittance of clouds. Theoretically and numerically it was shown that one obtains anomalous scaling for the transfer associated with optically thick fractal clouds. Since in the latter the exponent is

smaller than one, the scaling exponent for homogeneous clouds, the general features of heterogeneity is the tendency to make the atmosphere more transparent (and less reflective) compared to an equivalent uniform atmosphere. The same authors also showed that the diffusion approximation to the transport in optically thick fractal clouds may be poor: radiative transfer and diffusion may, but do not necessarily, yield the same anomalous transport exponents.

Note the basic distinction between optically thick and optically thin regimes. Assuming that the mean cloud density is equal to one, and the external scale of the cloud is equal one, the mass extinction coefficient κ_e can be used to characterize the optical thickness and the transfer properties. The mass extinction coefficient $\kappa_e = (1-g)\kappa_{dim}$ (where g is the asymmetry factor, $g=0$ for isotropic scattering) is the sum of the scattering coefficient κ_s and the absorption coefficient κ_a . However, in the following we will assume non-absorbing clouds, therefore the mass extinction coefficient is the cross section per unit mass of the scattering particles, the water droplets. When $\kappa_e \ll 1$ (the thin limit) the spatial variability of the cloud is unimportant, whereas when $\kappa_e \gg 1$ (the thick limit), it completely dominates the behavior and the homogeneous (plane parallel) and fractal results will be completely different, algebraically diverging as $\kappa_e \rightarrow \infty$. Since real clouds are at least moderately thick, it is obviously important that radiative transfer properties be inferred from cloud models with realistic scaling properties.

Many other researchers have now used fractal or multifractal cloud models for modeling radiative transport, although most results so far have been numerically derived. Cahalan 1989 has used Monte Carlo methods to study moderately thick ($\kappa_e \approx 1.5$) multifractal clouds allowing variability only in the horizontal: the optical depth was taken to be constant in vertical columns. In keeping with his modest thickness, he found small increases in transmittance (10-30%) compared to equivalent plane parallel models. These modest effects are reproduced in other thin cloud simulations using a different monofractal model called the "bounded cascade" model (Cahalan 1994). Similarly Barker and Davies 1992 have used thresholded two dimensional fractional Brownian motion monofractal clouds to model numerically (Monte Carlo) the overall albedoes of moderately thick cloud fields ($1.4 \leq \kappa_e \leq 7$). They investigated the bulk radiative response as a function of the scaling exponent of the models, finding highly significant effects associated with horizontal variability. Davis et al 1991 (see Davis et al 1993 for a summary) was the first to go beyond "bulk" flux estimates by numerically calculating detailed radiation fields. This was done on large (1024x1024) two dimensional multifractal cloud models using a class of universal multifractals (lognormal). For cross validation purposes both Monte

Carlo and relaxation techniques were used and the behavior was examined with κ_e increasing up to 200 (well into the optically thick regime).

Multifractal clouds have the realistic property of being highly variable even at fixed spatial scales. This means that obtaining reliable and efficient numerical algorithms to model the transfer is a nontrivial task. In order to overcome some of the limitations of both Monte Carlo and relaxation methods, Borde et al 1993 developed an accurate semi-implicit numerical scheme and used it to investigate the relation between the singularities in the radiation field and the cloud optical depth. Preliminary results include evidence that their multifractal indices were related to each other in a theoretically predicted way. Finally, by neglecting the correlations between more than two successive scatters, Evans 1993 has modified the backward Monte Carlo technique so as to obtain direct estimates of ensemble averaged optical properties of lognormal multifractal cloud fields. In the relatively thin clouds he studied ($\kappa_e=0.6, 1.5$), he found this approximation was quite accurate.

1.2 Outline

While the numerical approaches discussed above certainly provide indispensable tools for understanding radiation in scaling systems, in themselves they are insufficient to resolve the two basic physical problems: the statistical relationship between the radiation and cloud fields (as functions of resolution), and the scattering statistics describing the random trajectories of individual photons. While we have already mentioned some first steps in theoretically addressing the former, Lovejoy et al 1990 and Davis et al 1991 have obtained some initial results concerning the latter. Unfortunately, while their results (mostly direct transmittance statistics) apply to arbitrary multifractal clouds, they are only valid in the asymptotic limit involving small distances (in the notation to be introduced below, the large λ limit).

In this work, we overcome the limitations of this approach by considering asymptotically thick clouds; taking κ_e large and allowing the distances to extend over the entire available range. Although the results * will be specific to a special type of universal multifractal (the lognormal multifractals mentioned above), preliminary numerics indicate that the same type of approach can be considerably generalized. Furthermore, the large κ_e regime turns out to be attained for quite low κ_e (as low as 1-10), so that this does not appear to be a serious drawback. In any case, the extensive understanding of the scattering statistics obtained below sheds light on the basic processes involved.

* The basic results were announced in Lovejoy et al 1993.

We justify the model of a lognormal multifractal cloud model by analyzing cloud liquid water data. We are able to demonstrate an excellent scaling of the FIRE (First ISCCP Regional Experiment) data over the entire range of 5m-330km. Furthermore, we estimate the universal multifractal indices. These results inspire confidence that lognormal multifractals are indeed an appropriate model to describe real cloud liquid water content.

As the ultimate goal we try to provide a relationship between extremely variable random media, such as clouds, and the radiation field. A better understanding of this relationship is of fundamental importance for radiation budget calculations, climate models (Ramanathan et al. 1983, 1989), and among others, satellite imagery of clouds (Gabriel et al. 1988, Tessier et al 1993a).

The outline of this work is as follows: The next chapter establishes the basic theory of multifractals and radiative transfer as well as it develops our theoretical approach to describe the scattering statistics in multifractals. The results are checked in chapter 3 by numerical simulations and the range of validity is estimated. Our understanding of the scattering statistics leads in chapter 4 to a potential technique of renormalizing the multifractal clouds. It effectively reduces the multifractal transfer problem to a standard homogenous transfer problem, but with a drastically reduced "effective" extinction coefficient. We argue that this approximation will be even valid in the multiple scattering case and show how this result can be understood in the context of some recent results on diffusion in multifractals. Finally, in chapter 5, we analyze empirical cloud liquid water data with the aim to experimentally test the validity of the multifractal cloud model and to estimate the universal multifractal indices of real cloud data. All results of are then summarized in chapter 6.

2. Basic Theory

The object of this chapter is to establish the basic concepts of multifractals and radiative transfer which will then be used to develop the "singularity formulation of scattering in multifractals" which relates extremely variable random media, such as clouds, to the corresponding radiation field.

2.1 *Scaling and Fractal Dimension*

Before talking about multifractals it might be helpful to recapitulate the two essential ideas behind fractals: scaling symmetry and the fractal dimension. The easiest fractal one can think of is the Cantor set (1883), illustrated in figure 2.1. It is generated by starting off with the unit interval and iteratively removing middle (open) sets (leaving the endpoints as shown in the construction). When we apply this "cascade procedure" ad infinitum, we are left with a set of points $C = \lim_{k \rightarrow \infty} C_k$ (where C_k is the set at the k^{th} step), which is the Cantor set. Each piece of the set is, when enlarged appropriately, similar to the whole. This characteristic is called scale-invariant or simple *scaling*. Note that the self-similarity in the deterministic Cantor set is not a necessary requirement of scaling. In general, as most observations in nature show, when talking about scaling one rather thinks of statistically self-similar objects (e.g. coastlines, rivers, lightning).

Unfortunately in geophysics we are rarely interested in geometrical sets but usually much more interested in scalar fields (with values at each point) that arise in nature as a result of nonlinear processes. However, *fractal dimensions* are still useful in "counting the occurrence of a given phenomena". If the phenomena is scaling, then the number of occurrences $N_A(l)$ (at resolution l in space and/or time of a phenomena occurring on a set A) follows a power law* :

$$N_A(l) \approx \left(\frac{l}{L}\right)^{-D_F} \quad 2.1.1$$

where L is the fixed largest scale and D_F is the fractal dimension, generally not an integer, and is not to be confused with the topological dimension. So, for example, the fractal dimension of the Cantor set is $D_F = \frac{\log 2}{\log 3}$ whereas its topological dimension is $D_{\text{top}}=0$. Let us also define a fractal codimension c , which becomes important once we talk about multifractals. The codimension of a fractal set is simply the dimension of the embedding

* Here and below the sign \approx means equality within constants and slowly varying factors such as logarithms

space D (the topological dimension of the space in which the fractal is embedded, e.g. for the Cantor set $D=1$) minus the fractal dimension: $c=D-D_F$.

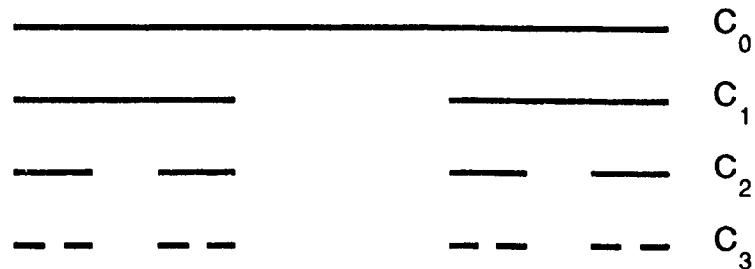


Figure 2.1: The first three iteration steps of the construction of the Cantor set.

2.2 Multifractal Clouds

Geophysical scalar fields including cloud fields (chapter 5 below, Tessier et al. 1993a), temperature and wind fields (Schmitt et al. 1992, Schmitt 1992), rain (Lovejoy et al 1987, Tessier et al 1993a), topography (Lavallée et al. 1993), as well as ice (Francis et al 1994), pollution (Salvadori et al 1993) and the roughness of the ocean surface (Tessier et al. 1993b), have been analyzed over various time and scales and have been shown to be multifractal in nature. The multifractal models used here were first developed as phenomenological models of turbulent cascades. Presumably in hydrodynamic turbulence, the governing nonlinear dynamical (Navier-Stokes) equations have three basic properties that lead to the cascade phenomenon: 1) scaling symmetry, 2) a quantity conserved by the cascade (energy fluxes from large to small scale), and 3) localness in Fourier space (i.e. the dynamics are most effective between neighboring scales). Cascade models are relevant in the atmosphere and in particular in clouds since the underlying dynamics is of hydrodynamic turbulent origin. There is now a whole series of such phenomenological models: the "pulse-in-pulse" model (Novikov and Stewart 1964), the lognormal model (Kolmogorov 1962; Obhukhov 1962; Yaglom 1966), the weighted-curdling model (Mandelbrot 1974), the β -model (Frisch et al. 1989), the α -model (Schertzer and Lovejoy 1983), the random β -model (Benzi et al. 1984), the p -model (Meneveau and Sreenivasan 1987), and the continuous universal cascade models (Schertzer and Lovejoy 1987b).

The key assumption in these phenomenological models of turbulence is that successive steps define the fraction of the flux of the liquid-water density distributed over small scales. Note that it is clear that the small scales cannot be regarded as adding

density, they only modulate the density passed down from larger scales. The hypothesis is that the fraction of the density flux from the parent structure to an offspring is distributed in a scale invariant way. If the resulting scaling field cannot be characterized by a unique fractal geometric set, but by an infinite hierarchy of them, it is called a *multifractal* (a term coined by Parisi and Frisch 1985).

This cascade procedure is easy to illustrate in the so called "discrete cascade models" where the scales are discretized and a discrete multiplicative process determines the density ρ_λ (at scale λ^{-1}) (Figure 2.2). A large structure of characteristic length equal to x_0 and density ρ_0 equal to 1 is broken up into smaller substructures of characteristic length $x_1 = x_0/\lambda_0$ ($\lambda_0 = 2$ is the scale ratio between two consecutive steps in this particular example). The density in each substructure is multiplicatively modulated by a random factor (keeping the overall ensemble average fixed $\langle \rho_\lambda \rangle = 1$). When this process is repeated (the overall ratio λ is increased) larger and larger values of ρ_λ appear, concentrated on a smaller and smaller length. In the small scale limit, the result is highly variable.

In this place we want to clarify the dimensions of the most frequently used variables in this text: In the following mostly the nondimensional variables (λ , x , ρ , κ , τ_p) will be used:

<i>variable</i>	<i>dimension</i>	<i>physical interpretation</i>
L	m	external scale of the cloud
l	m	distance within the cloud
$x = l/L$	-	nondimensional distance within the cloud
$\lambda = L/l$	-	Scale ratio corresponding to l
Λ	-	largest scale ratio of the cascade, corresponding to the resolution of cloud variability
$\rho_{dim}(x)$	kg/m ³	liquid-water (LW-) density at a point x in the cloud
$\rho(x) = \frac{\rho_{dim}(x)}{\langle \rho_{dim}(x) \rangle}$	-	nondimensional LW-density at a point x in the cloud
κ_{dim}	m ² /kg	mass extinction coefficient
$\kappa = \kappa_{dim} \langle \rho_{dim} \rangle L$	-	nondimensional extinction coefficient. In this work it is the nondimensional coupling constant between the cloud and the radiation field, i.e. matter and radiation
$\lambda_{dim} / \langle \rho_{dim} \rangle$	m	mean free path; typical physical distance per scatter in the corresponding inhomogeneous cloud
τ_p $= \kappa x = l \kappa_{dim} \langle \rho_{dim} \rangle$	-	photon path distance nondimensionalized by the mean free path, i.e. the distance measured in mean free paths

Table 2.1: Dimension and physical interpretation of variables

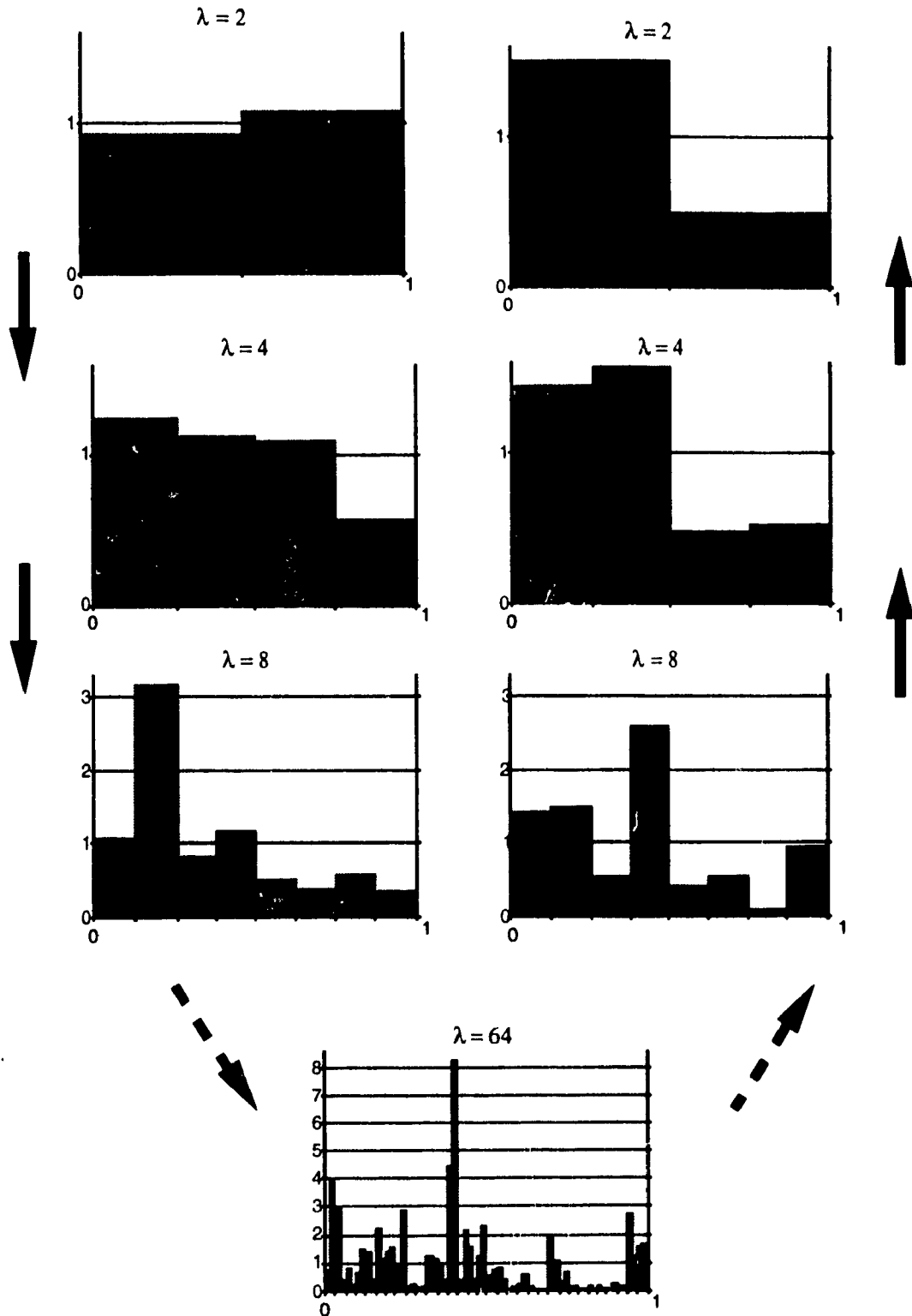


Figure 2.2: The left hand side shows the step by step construction of the "bare" multifractal cascade (α -model) starting with an initial uniform density. At each step the horizontal scale is divided by two, and independent random factors are chosen either <1 or >1 , normalized to ensure that $\langle \rho_\lambda \rangle = 1$. The largest scale ratio is $\Lambda = 64$. The right hand side shows the effect of integrating over larger and larger scales and yields a "dressed" cascade.

The multiple scaling properties of a process, measured at a scale $x=\lambda^{-1}$, can be described by two complementary approaches:

The first examines the probability distribution. In the scaling regime λ , the measures ρ_λ have the property (Schertzer and Lovejoy 1987b):

$$\Pr(\rho_\lambda \geq \lambda^\gamma) \approx \lambda^{-c(\gamma)} \quad 2.2.1$$

where γ is the order of singularity. Therefore $c(\gamma)$ is a scaling exponent of the probability distribution. When the dimension of the embedding space D is larger than the probability distribution exponent $c(\gamma)$ we may introduce the dimension function $D(\gamma) = D - c(\gamma)$. It is simply the fractal dimension of the set of density measures ρ_λ exceeding the threshold λ^γ (Figure 2.3).

The other equivalent approach to describe the multifractal field is to specify the scaling of the statistical moments $\langle \rho_\lambda^q \rangle$. We define the multiple-scaling exponent $K(q)$:

$$\langle \rho_\lambda^q \rangle \approx \lambda^{K(q)}, \quad \lambda > 1 \quad 2.2.2$$

where q is the moment. The moment exponent $K(q)$ is related to the probability distribution exponent $c(\gamma)$ by the following Legendre transformation (Parisi and Frisch 1985):

$$\begin{aligned} K(q) &= \max_\gamma [q\gamma - c(\gamma)] \\ c(\gamma) &= \max_q [q\gamma - K(q)] \end{aligned} \quad 2.2.3$$

which implies a one to one relationship between orders of singularities and moments:

$$\begin{aligned} \gamma &= K'(q) \\ q &= c'(\gamma) \end{aligned} \quad 2.2.4$$

To fully specify the multiple scaling of the fields an infinite number of scaling parameters, e.g. the entire $K(q)$ or $c(\gamma)$ function, will be required. However, we will use universal multifractals corresponding to stable attractive behaviors of multifractal processes. Multifractals of this universality class can be characterized by only three parameters (α, C_1, H) . These are: the Lévy index, the codimension of the mean, and the deviation of the observed field from the conserved field. The Lévy index α indicates the class to which the probability distribution belongs; it tells us about the degree of

multifractality ($0 \leq \alpha \leq 2$, $\alpha=0$ corresponds to a monofractal). The parameter C_1 is the fractal codimension of the field thresholded at the mean value of the field, it tells us about the sparsity of the average level of intensity. Figure 2.3 illustrates the fractal codimension of a field thresholded at a value equal to λ^γ . Parameter H measures the degree of nonstationarity in the process; it is a measure of the conservation of the field over different scales, e.g. $H=0$ is a conserved or stationary multifractal.

For universal multifractals the two scaling exponents of the probability distribution and the moments are following functions:

$$c(\gamma) = C_1 \left(\frac{\gamma}{C_1 + \alpha} + \frac{1}{\alpha} \right)^{\alpha} \quad 2.2.5a$$

$$K(q) = \frac{C_1}{\alpha-1} (q^\alpha - q) \quad 2.2.5b$$

with $0 < \alpha \leq 2$, $\alpha \neq 1$ and $\frac{1}{\alpha} + \frac{1}{\alpha} = 1$. For lognormal multifractals ($\alpha=2$) this reduces to:

$$c(\gamma) = \frac{C_1}{4} \left(\frac{\gamma}{C_1} + 1 \right)^2 \quad 2.2.6a$$

$$K(q) = C_1 (q^2 - q) \quad 2.2.6b$$

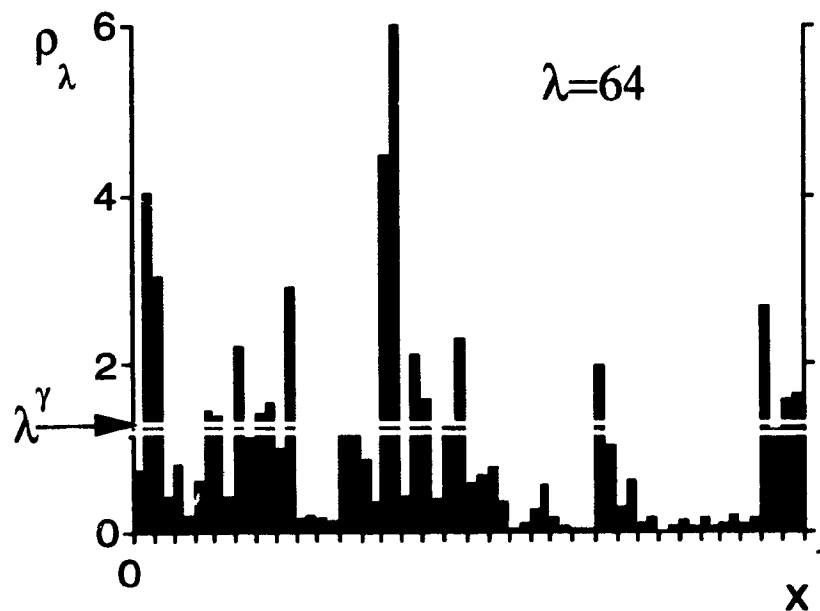


Figure 2.3: 1-dimensional lognormal multifractal cloud field analyzed over a scale ratio $\lambda=64$. There is a threshold on the field at the density $\rho_\lambda = \lambda^\gamma$ corresponding to the order of singularity γ . The fractal dimension of the set of density measures ρ_λ exceeding this threshold (cut in the graph) is given by the function $D(\gamma) = 1 - c(\gamma)$.

2.3 Bare and Dressed Multifractals

In multifractal theory it is important to distinguish between the "bare" and the "dressed" quantities (Schertzer and Lovejoy 1987a). The bare quantity is obtained after the cascade generating the cloud field has proceeded down to scale λ . The corresponding dressed quantity is obtained after integrating the completed cascade over the same scale (Figure 2.2 above). This implies that the bare quantities have no small scale interactions, whereas the dressed ones have a full range of interactions. A cascade whose development is limited to the scale Λ is "bare" on this scale: no smaller activity is hidden or "dressed".

We calculate the average transmission $\langle T(x) \rangle$ by considering the bare cloud density field ρ_λ at scale $x = \lambda^{-1}$, since its probability distribution is known analytically (eq. 2.5.7). Furthermore the bare/dressed difference of the fields is a random factor of the order 1 for the non-extreme events* (low values of ρ , γ) and therefore does not affect the scaling. The dressed density whose low order exponents (of interest here) are the same as those of the bare at the distance $x = \lambda^{-1}$ is calculated as

$$\rho_{\lambda,d}(x) = \frac{\int_0^1 \rho_\Lambda(x') dx'}{\int_0^1 dx'} \quad 2.3.1$$

where ρ_Λ is the density at the smallest scale Λ^{-1} (scale of resolution). The difference arises for high order of moments q larger than a critical order of moment q_D beyond which all the dressed moments diverge, $\langle \rho_d^q \rangle \rightarrow \infty$ for $q > q_D$. The corresponding probability distributions of the bare/dressed fields are the same (to within slowly varying and constant factors) for the order of singularity γ smaller than γ_D where γ_D is the critical singularity corresponding to q_D ($\gamma_D = K'(q_D)$, eq. 2.2.4). For $q > q_D$, $\gamma > \gamma_D$, the corresponding $K(q)$ and $c(\gamma)$ functions have discontinuities in their derivatives of various order. Due to a formal analogy with thermodynamics, these are called "multifractal phase transitions" (for further details see Schertzer and Lovejoy 1987a).

* The difference is the "hidden" factor which is of order one for small values, but which diverges for orders of singularities γ larger than a critical value γ_D ; see Schertzer et al 1993.

2.4 The Equation of Radiative Transfer

Although we will not make direct use of the radiative transfer equation in the following it is important to relate our approach to this fundamental equation. Whereas here we just give a very concise summary, there are numerous books written on the topic (e.g. Chandrasekhar 1960) which discuss many conceivable viewpoints but say little about the horizontally heterogeneous case of interest to us.

For an arbitrary geometry the radiative transfer equation (without frequency dependence) takes the form:

$$\vec{\Omega} \cdot \vec{\nabla} I(\vec{r}, \vec{\Omega}) = -\kappa_{\text{dim}} \rho(\vec{r}) [I(\vec{r}, \vec{\Omega}) - J(\vec{r}, \vec{\Omega})] \quad 2.4.1$$

plus boundary conditions. $I(\vec{r}, \vec{\Omega})$ is the radiance or specific intensity at a point defined by the vector \vec{r} and for radiation propagating in direction $\vec{\Omega}$. κ_{dim} is the mass extinction coefficient and $\rho(\vec{r})$ is the density of the material (e.g. liquid water content). $J(\vec{r}, \vec{\Omega})$ defines the so called source function which has following form:

$$J(\vec{r}, \vec{\Omega}) = \frac{\omega_0}{4\pi} \int p(\vec{r}, \vec{\Omega}, \vec{\Omega}') I(\vec{r}, \vec{\Omega}') d\Omega' + J_s(\vec{r}, \vec{\Omega}) \quad 2.4.2$$

ω_0 is the albedo for single scattering, $p(\vec{r}, \vec{\Omega}, \vec{\Omega}')$ defines the phase function characterizing the scattering in the direction $\vec{\Omega}$ of radiation arriving from the direction $\vec{\Omega}'$ on a volume element at point $\vec{\Omega}$. The phase function is normalized with $\int p(\vec{r}, \vec{\Omega}, \vec{\Omega}') d\vec{\Omega}' = 4\pi$. Finally $J_s(\vec{r}, \vec{\Omega})$ is a term arising from internal or external sources of radiation or both.

In the following we assume no internal nor external sources of radiation (except the incident radiation on top of the cloud). Since we are concerned about the direct transmission $T(x)$ in a one dimensional path through the cloud, light scattered into the path is not considered, therefore the source function $J(\vec{r}, \vec{\Omega})$ becomes zero. We are left with a homogeneous linear differential equation:

$$\frac{dI(x)}{dx} = -\kappa_{\text{dim}} \rho(x) I(x) \quad 2.4.3$$

with the solution:

$$T(x) = I(x) = I(0) \cdot e^{-\kappa_{\text{dim}} \int_0^x \rho(x) dx} \quad 2.4.4$$

We recognize the exponent as the optical depth. In the following, by defining the incident radiation $I(0)$ equal to one, we can choose a stochastic interpretation, which physically corresponds to the photon representation of light.. Equivalent to the direct transmission we talk about the probability that a random photon distance x' between two consecutive scatters exceeds a distance x , the actual distance in the cloud. The standard photon free path probability distribution is then defined as:

$$\Pr(x' > x) = T(x) = e^{-\tau(x)} \quad 2.4.5$$

Figure 2.4 illustrates 1-dimensional "random photon walks" in various conserved lognormal multifractal clouds ($\alpha=2$, $H=0$) with (i.e. the extinction coefficient varies between $\kappa=32$ and $\kappa=128$ and the codimension of the mean of the multifractal cloud C_1 varies between $C_1=0.1$ and $C_1=0.9$). As one would expect, with increasing extinction coefficient κ the mean free path length of the photon decreases. Notice also the change of the sparsity of the field due to changes of C_1 . In chapter 5 we will analyze cloud liquid-water-content data and find that the clouds can be described by lognormal multifractals with $C_1 \approx 0.08$, but with $H \approx 0.3$.

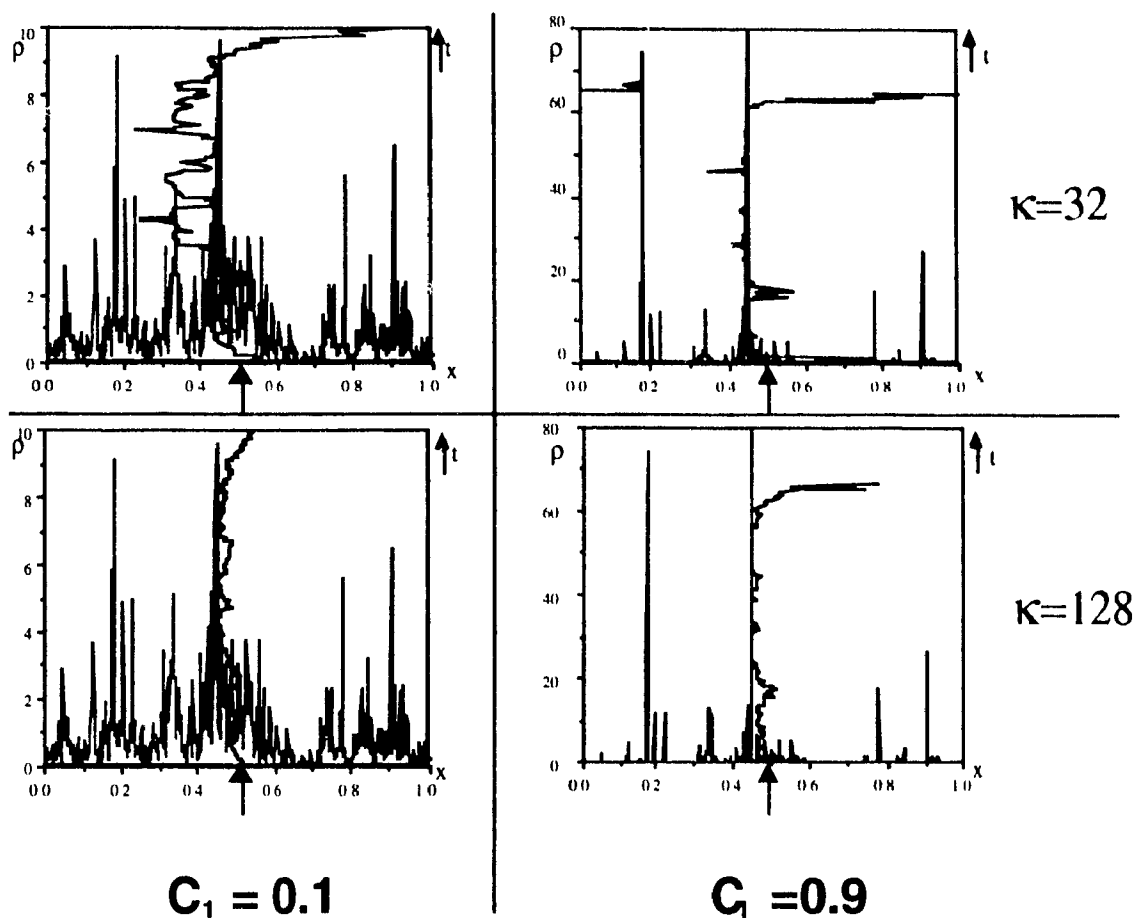


Figure 2.4 Monte Carlo simulations of a photon "random walk" in different multifractal clouds. In each graph we plotted the 1-d density field (resolution $\Lambda^{-1}=1/512$) and the photon random walk. The photon enters the cloud at the middle of the cloud (shown by the arrow) and moves either to the left or the right (with the same probability). The x-axis represents the position in the cloud, whereas the y-axis represents the cloud density as well as the "time" of the walk (units arbitrary). The simulated clouds on the left/right side have a codimension of the mean $C_1=0.1/C_1=0.9$. Note that a higher codimension of the mean results in a sparser field (with higher density spikes!). The simulated clouds in the upper row have an extinction coefficient of $\kappa=32$, and the clouds in the lower row have an extinction coefficient of $\kappa=128$. As expected, the mean free path length of the photon decreases with increasing extinction coefficient. Note also the periodic boundary conditions: in the upper right graph the photon left the cloud on the right side and reentered the cloud on the left.

2.5 Singularity Formulation of Scattering in Multifractal Clouds

To describe the photon free path distribution we adopt the formalism of the above described multifractal theory (section 2.2). Therefore we map ρ_λ to the dimensionless photon path distance τ_p and write it as a function scaling with an order of singularity γ_p :

$$\tau_p = \kappa x = \kappa^{\gamma_p} \quad 2.5.1$$

Note that τ_p , the dimensionless photon path distance, is not to be confused with the optical depth τ . The nondimensional extinction coefficient κ takes the place of the scaling parameter λ . For simplicity reason, we will no longer require a distinction between κ_{dim} and κ_e since they just differ by a constant. Instead of the probability distribution exponent $c(\gamma)$ of the cloud density (as a function of the order of singularity γ) we now talk about a probability distribution exponent $c_p(\gamma_p)$ of the photon path distribution (as a function of the order of photon path singularity γ_p). So we write the free photon path probability distribution (compare to eq. 2.2.1) as:

$$\langle T \rangle = \text{Pr}(\tau_p \geq \kappa^{\gamma_p}) \approx \kappa^{-c_p(\gamma_p)} \quad 2.5.2$$

By the same token we use the multifractal formalism to describe the scaling of the moments of the free photon path distribution (compare to eq. 2.2.2)

$$\langle \tau_p^q \rangle \approx \kappa^{K_p(q)} \quad 2.5.3$$

and anticipate that the two will be linked by a Legendre transform as in the standard multifractal case.

In order to calculate the transmission through the cloud we remember that the distance x corresponds to a scale, $x=\lambda^{-1}$, at which the bare density ρ_λ is constant: $\rho_\lambda = \lambda^\gamma$. Therefore the optical depth (eq. 2.4.4) is simply the cloud density multiplied by the nondimensional extinction coefficient and the distance: $\tau(x) = \kappa \lambda^\gamma \lambda^{-1}$. We are now able to calculate the mean transmission through a distance $x=\lambda^{-1}$ averaged over singularities of the order γ :

$$\langle T(\lambda^{-1}) \rangle = \int_{-\infty}^{\infty} e^{-\tau(\gamma)} p(\gamma) d\gamma \quad 2.5.4$$

where the optical depth $\tau = \kappa \rho_\lambda x = \kappa \lambda^\gamma \lambda^{-1} = \kappa \lambda^{\gamma-1} = \kappa^{\gamma\tau}$. The last equality in the previous expression defines γ_τ . Since we will be interested in κ large, but not necessarily λ large, we make the following transformation of variables:

$$\gamma = 1 - \frac{(1 - \gamma_\tau)}{(1 - \gamma_p)} \quad 2.5.5$$

and obtain:

$$\langle T(\lambda^{-1}) \rangle = \int_{-\infty}^{\infty} e^{-\kappa^{\gamma\tau}} p\left(1 - \frac{1 - \gamma_\tau}{1 - \gamma_p}\right) d\gamma_\tau \quad 2.5.6$$

The further calculations for general multifractals will be given in future publications, the results are given below. Here we treat the universal lognormal multifractal case for which the probability density of the (bare) lognormal multifractal density field $\rho_\lambda = \lambda^\gamma$ is explicitly given:

$$p(\gamma) = \sqrt{\frac{\log \lambda}{4C_1\pi}} e^{-\frac{\log \lambda}{4C_1}(\gamma + C_1)^2} \quad 2.5.7$$

and we write the integral 2.5.6:

$$\langle T(x) \rangle = \sqrt{\frac{\log \kappa}{4C_1\pi(1 - \gamma_p)}} \int_{-\infty}^{\infty} e^{-\frac{\log \kappa}{4C_1(1 - \gamma_p)}[(1 - \gamma_\tau) - (1 + C_1)(1 - \gamma_p)]^2} e^{-\kappa^{\gamma\tau}} d\gamma_\tau \quad 2.5.8$$

There are now two ways to proceed. Perhaps the clearest way mathematically is to determine the Laplace transform of $\langle T(x) \rangle$ which yields the moment scaling exponent $K_p(q)$ in equation 2.5.3 via an exact calculation (see Appendix A1). The alternative is to obtain the probability distribution exponent $c_p(\gamma_p)$ (Appendix A2) by directly approximate eq. 2.5.8 and then take the Legendre transform of the result. In either case, we obtain:

$$K_p(q) = q - \frac{1}{2C_1} \left(\sqrt{(1 + C_1)^2 + 4C_1q} - (1 + C_1) \right). \quad 2.5.9$$

This is an essential result and will allow us to approximate the overall transmission by renormalizing the extinction coefficient (chapter 4). First, however, we return to the

ensemble averaged transmission function and determine the probability distribution exponent of the photon path distribution, $c_p(\gamma_p)$. We take the Legendre transform of the moment scaling function of eq. 2.5.9:

$$c_p(\gamma_p) = \max_q (q\gamma_p - K_p(q)) \quad 2.5.10$$

which yields a maximum for: $\gamma_p = K'(q) = 1 + ((1 + C_1)^2 + 4C_1q)^{-1/2}$. Making this substitution results in:

$$c_p(\gamma_p) = \frac{(1 - (1 + C_1)(1 - \gamma_p))^2}{4C_1(1 - \gamma_p)} \quad 2.5.11$$

This result is consistent with using the Laplace method (see Appendix A2) for the integral 2.5.8: in the limit of large κ evaluate the integral with $\gamma_r \approx 0$. This asymptotic result valid for large κ establishes a one to one relation between orders of singularity in the cloud field γ and orders of singularity in the photon path statistics: $\gamma_p \approx \frac{\gamma}{\gamma-1}$ with $\gamma < 1$ (eq. 2.5.5). The strong cloud density singularities $\gamma > 1$ represent such a high cloud density that they play no role. The moderate cloud density singularities $0 < \gamma < 1$ contribute to the regularities ($\gamma_p < 0$) in the photon statistics. On the other hand the cloud density regularities ($\gamma < 0$) determine the singularities ($\gamma_p > 0$) in the photon statistics (see Figures 2.5, 2.6).

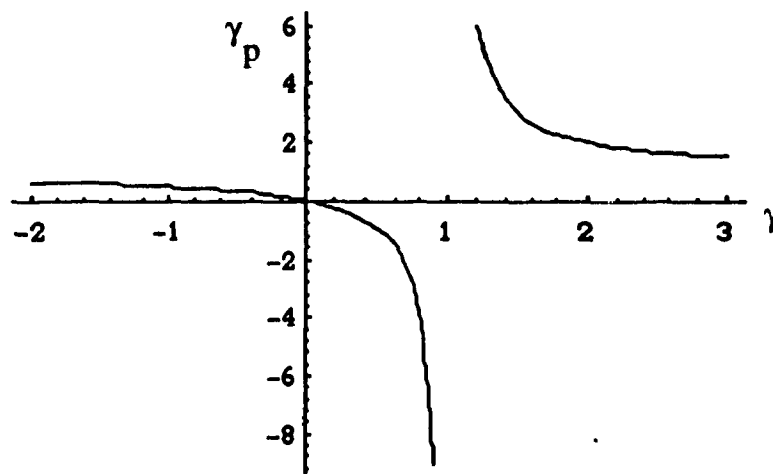


Figure 2.5: A graph of $\gamma_p = \frac{\gamma}{\gamma-1}$ (obtained with $\gamma_r=0$) showing the physical branch (left), and unphysical branch (right).

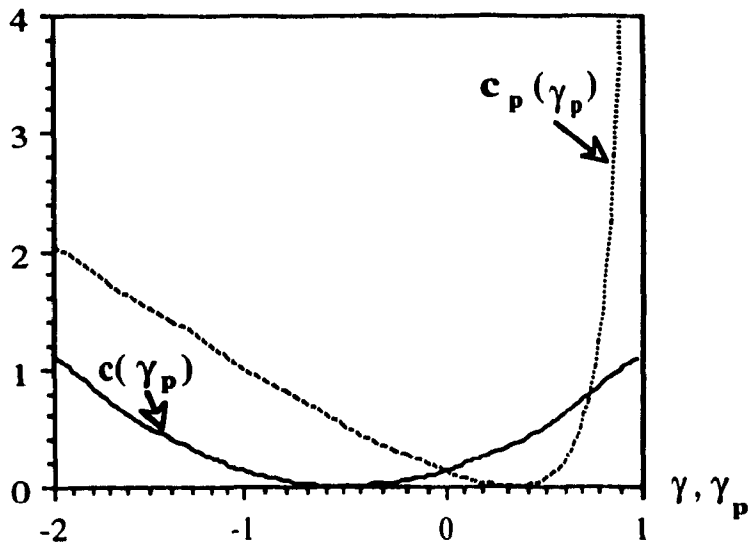


Figure 2.6: Comparison of the cloud density probability distribution exponent $c(\gamma)$ with the corresponding bare free path distribution exponent $c_p(\gamma_p)$. The codimension of the lognormal multifractal cloud was chosen as $C_1=0.5$, which corresponds to a minimum of the probability distribution exponent $c(\gamma)$ at $\gamma=-C_1=-0.5$.

In the case of general multifractals integral 2.5.6 can be approximated if the probability distribution exponent $c(\gamma)$ satisfies the condition $c'(\gamma)<0$ for small γ . One yields the following free path probability distribution exponent:

$$c_p(\gamma_p) = c\left(1 - \frac{1}{1-\gamma_p}\right)(1 - \gamma_p) \tag{2.5.12}$$

The moment scaling exponent can then be obtained by Legendre Transformation.

3. Numerical Simulations and Dressed Statistics

The goal of this part is to show, that the analytical bare approach of chapter 2 yields results consistent with the actual physical process. A photon traveling through a cloud interacts with the cloud water/ice droplets at smallest scale, independent of how big the free path length will be. We therefore simulate lognormal multifractal clouds and the photon transport through these clouds, obtaining a transmission function $T(x)$. Analyzing these findings by two different multifractal analysis techniques, leads to the "dressed" probability distribution exponent $c_{p,d}(\gamma_p)$ and the moment scaling exponent $K_{p,d}(q)$, which we compare to the analytically bare results.

3.1 Simulating the Multifractal Clouds

To compare the "bare" approximation developed above with the dressed statistics we will simulate the transport through multifractal fields. To do this, the lognormal multifractal clouds are simulated by a continuous cascade algorithm (Schertzer and Lovejoy 1987b) which we briefly summarize. First we define the generator $\Gamma_\lambda = \log \rho_\lambda$. To yield a multifractal ρ_λ field the generator must be exactly a $1/f$ noise, that is, its generalized spectrum is $E(k) \approx k^{-1}$ (this is necessary to ensure the multiple scaling of the moments of ρ_λ). To produce such a generator, we generate a stationary gaussian noise whose amplitude is determined by the codimension of the mean C_1 . The resulting noise is fractional integrated (power-law filtered in Fourier space) to give the desired k^{-1} spectrum. Finally, the result is exponentiated to give ρ_λ , which will thus depend on C_1 . Because of the fractional integration the entire process evolves two FFTs. Simulations were performed using three C_1 different codimensions of the mean, $C_1=0.1$, $C_1=0.5$, $C_1=0.9$, corresponding to increasingly violent fluctuations in the cloud model. Note that real cloud liquid-water content fields have parameters estimated to be roughly $\alpha \approx 2$, $C_1 \approx 0.08$, $H \approx 0.3$ (chapter 5).

3.2 Simulating the Transport

For the numerical simulations of the transport we simply discretize the optical depth integral (2.4.4) and calculate the ensemble averaged transmission as a function of path length $\tau_p = \kappa x$:

$$\langle T(\tau_p) \rangle = \left\langle e^{-\kappa \sum_i \rho_\Lambda(\tau_i) \Lambda^{-1}} \right\rangle \quad 3.2.1$$

The simulated multifractal cloud density field $\rho_\Lambda(x_i)$ had the resolution (scale of homogeneity) Λ^{-1} , with an overall optical depth of κ (since $\langle \rho_\Lambda \rangle = 1$ and the external scale equal unity). To calculate the transmission through one realization (Fig. 3.1) the photon starting points inside the cloud were randomly chosen. Moreover, we implemented periodic boundary conditions and calculated the transmission for $0 < \tau_p < \kappa$. Finally the ensemble average was taken over the total number of realizations. This procedure was repeated for increasing nondimensional extinction coefficients $\kappa = 2^n$; $n=1,2,\dots,10$. Figure 3.1 illustrates the numerical transport model.

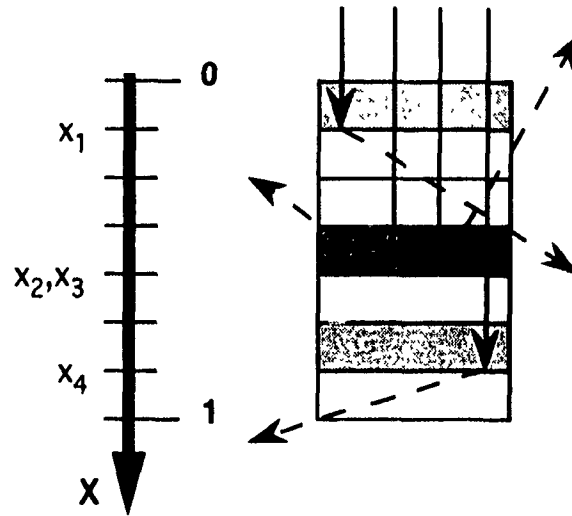


Figure 3.1: Schematic view of the numerical transport model. The scale of resolution for this simulated cloud is $\Lambda^{-1}=1/7$. Each element has a certain density ρ_Λ (the darkness of the fields corresponds to the density). All photon starting points are at the beginning of the cloud. The cells with a higher density have a higher probability of scattering the photons.

3.3 The Probability Distribution Exponent

In order to obtain the dressed probability distribution exponent $c_{p,d}(\gamma_p)$ for the simulated data we used the "Probability Distribution/Multiple Scaling" technique (PDMS) (Lavallée et al 1991a, Lavallée 1991). The method consists of directly exploiting the scaling of the dressed probability distribution:

$$\Pr(\tau_p \geq \kappa^{\gamma_p}) \approx \kappa^{-c_{p,d}(\gamma_p)} \quad 3.3.1$$

The technique is distinguished from other histogram based techniques (e.g. Paladin and Vulpiani 1987, Atmanspacher et al. 1989) in that they overcome the nontrivial problem of the (slowly varying) proportionality constants in the above equation, by examining the histograms over a range of scales rather than a single scale. The drawback of these methods is that they are sensitive to the correct normalization of the fields: the ensemble average of the overall transmission must be close to zero (see 3.4a) for further discussion).

First the logarithm of the probability distribution is plotted versus the logarithm of κ for each fixed order of singularity γ_p . We analyzed the probability distribution for photon path lengths exceeding the threshold κ^{γ_p} : $\Pr(\tau_p > \kappa^{\gamma_p})$, as well as the probability distribution for photon path lengths below the threshold κ^{γ_p} : $\Pr(\tau_p < \kappa^{\gamma_p})$ (Figure 3.2 and 3.3). If the probability distributions obey equation (3.3.1), these points lie on a straight line, whose absolute slope is the dressed probability distribution exponent $c_{p,d}(\gamma_p)$. In Figure 3.3 and 3.5 we compare the now obtained dressed probability distribution exponent $c_{p,d}(\gamma_p)$ with the analytical derived bare probability distribution exponent $c_p(\gamma_p)$ (eq. 2.5.11). Note the two distinct curves for the dressed probability distribution exponent: The probability distribution $\Pr(\tau_p > \kappa^{\gamma_p})$ leads to the right rising branch whereas the probability distribution $\Pr(\tau_p < \kappa^{\gamma_p})$ leads to the left branch of $c_{p,d}(\gamma_p)$.

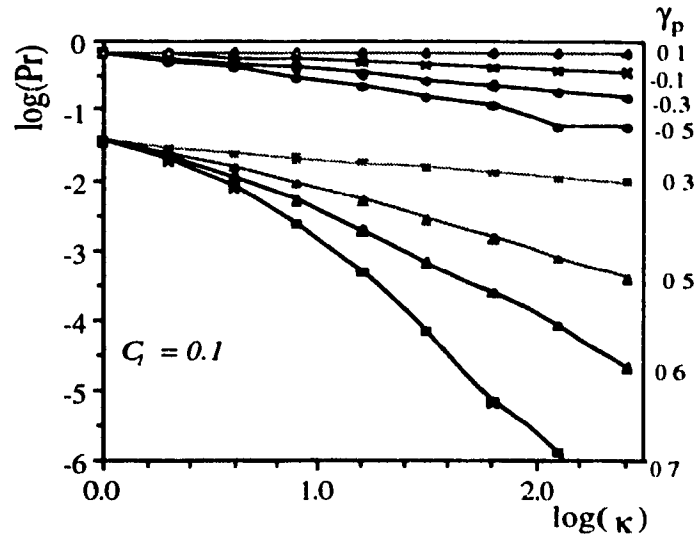


Figure 3.2: PDMS analysis of the free-photon path length probability distribution. Simulation with $\alpha=2$, $C_1=0.1$, scale ratio of homogeneity $\Lambda=4096$, 1000 realizations, 512 photon-starting points in each realization. The upper 4 lines represent $\log_{10} \Pr(\tau_p < \kappa^{\gamma_p})$ whereas the lower 4 lines represent $[\log_{10} \Pr(\tau_p > \kappa^{\gamma_p})] - 1$ versus $\log_{10}(\kappa)$. The scaling holds down until $\log_{10}(\kappa)=0.6$ as indicated in the text (low κ breakdown). For $\gamma_p < -0.3$ and $\gamma_p > 0.6$ the scaling is not provided anymore which is in good agreement with the of theoretically predicted limits ($\gamma_p^{\min} = -0.33$, $\gamma_p^{\max} = 0.6$).

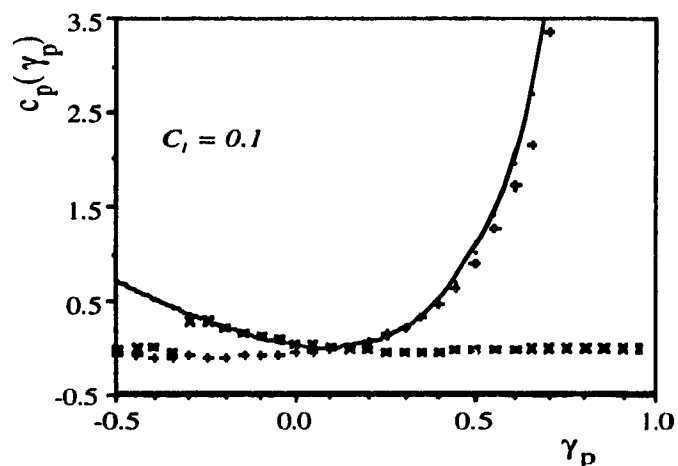


Figure 3.3: Comparison of the analytically derived bare $c_p(\gamma_p)$ -function with the numerically derived $c_{p,d}(\gamma_p)$ function obtained from the slopes in the previous graph (in the range $8 \leq \kappa \leq 256$). In the predicted range of validity $\gamma_p^{\min} = -0.33 < \gamma_p < 0.6 = \gamma_p^{\max}$ there is a good agreement between both curves. The left branch represents $\Pr(\tau_p < \kappa^{\gamma_p})$ and the right branch represents $\Pr(\tau_p > \kappa^{\gamma_p})$.

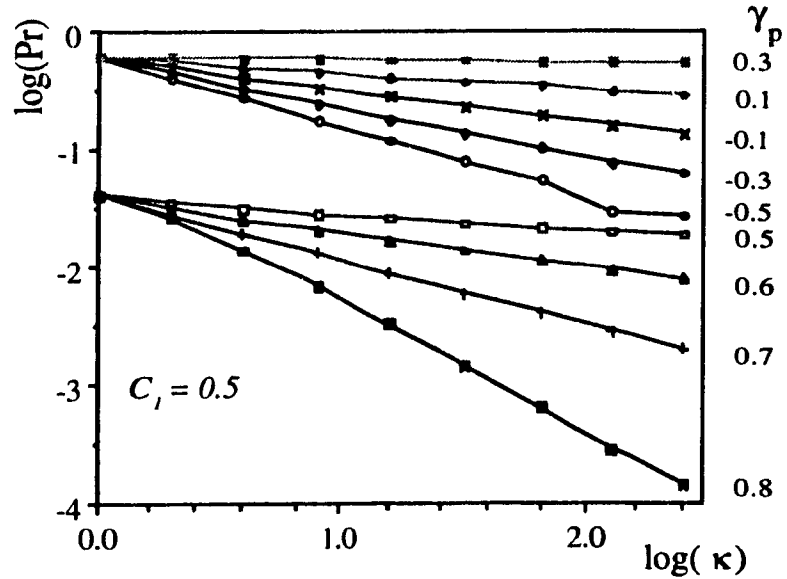


Figure 3.4: As figure 3.2 just with $C_1=0.5$. Here the scaling holds down until $\log_{10}(\kappa)\approx 0.9$. For $\gamma_p < -0.3$ and $\gamma_p > 0.8$ the scaling is not provided anymore which is in good agreement with the of theoretically predicted limits ($\gamma_p^{\min} = -0.33$, $\gamma_p^{\max} \approx 0.8$).

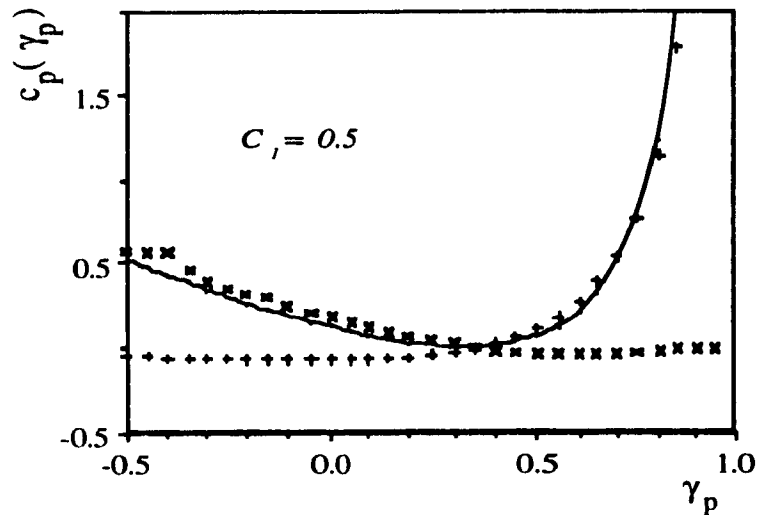


Figure 3.5: As figure 3.3 just with $C_1=0.5$. In the predicted range of validity $\gamma_p^{\min} = -0.33 < \gamma_p < 0.8 = \gamma_p^{\max}$ there is a good agreement between both curves.

3.4 Limits of Validity for the Probability Distribution Exponent

a) Breakdown for low extinction coefficients

As mentioned in the previous chapter, the bare analytical result for the probability distribution exponent $c_p(\gamma_p)$ was calculated by assuming a large nondimensional extinction coefficient κ . Here we want to estimate the lowest κ at which the bare result actually holds.

A low extinction coefficient κ implies that the average transmission $\langle T(x) \rangle$ at the largest scale $x=1$ is still reasonably high i.e. it cannot be approximated as zero (physically this corresponds to a transparent cloud). Therefore the free photon path distribution is not normalized anymore, which results in a breakdown of the scaling in the PDMS graphs at small extinction coefficients. Figure 3.2 and 3.4 show this behavior for extinction coefficients smaller $\log \kappa \approx 0.6 (C_1=0.1)$ and $\log \kappa \approx 0.9 (C_1=0.5)$. The bare result however, has a total transmission equal zero, independent of the extinction coefficient κ . This can be easily derived from equation 2.5.11: For $\gamma_p=1$, which corresponds to a actual photon path length equal to one, the probability distribution exponent c_p is equal minus infinity, which corresponds to zero transmission ($x=1 \Rightarrow \gamma_p=1$, $c_p = -\infty \Rightarrow \langle T \rangle = 0$).

We use this bare/dressed difference of the total transmission to estimate the lowest κ for which the bare approximation holds. An estimate of the lowest extinction coefficient κ_{\min} at which the total transmission differs significantly from zero can be given by the following formula.

$$\kappa_{\min} = |\log F|^{1+C_1} \quad 3.4.1$$

where F is the average transmission at largest scale $F = \langle T(1) \rangle$. This can be derived from the renormalization approach (see chapter 4). Figure 3.6 illustrates this estimation of the lowest extinction coefficient.

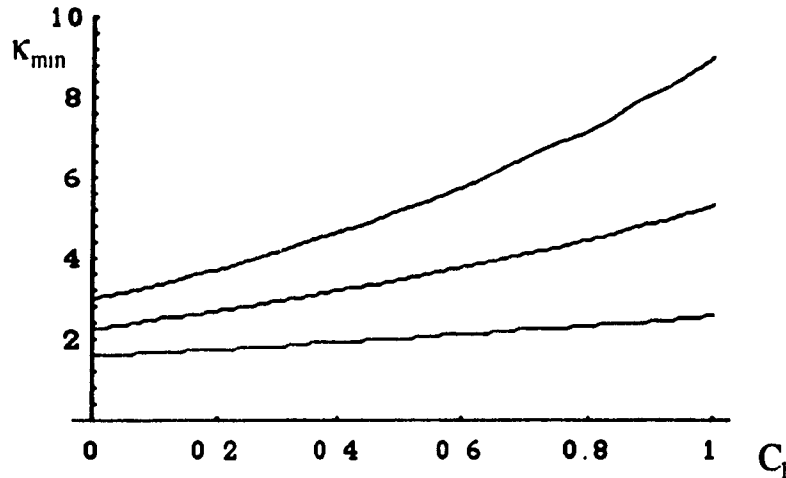


Figure 3.6: Estimates of the minimum extinction coefficient (κ_{min}) over which the asymptotic theory is expected to hold based on $F=20\%$, 10% , 5% (top to bottom) direct transmission through the cloud using the renormalization formula (below)

b) Limits on the Range of Photon Path Length Singularities

The other limit on the above estimated dressed probability distribution exponent arises due to a limited range of photon path distances (corresponding to photon path singularities γ_p) which we were able to estimate. An examination of the simulated cloud fields will help to answer this question. The simulated cloud fields underlie two basic limitations:

(1) The simulated clouds are generated up to a finite resolution Λ^{-1} . At this scale of resolution the cloud has a constant density ρ_Λ , it is homogeneous. Since in a homogeneous medium the mean free path is κ^{-1} , we require $\kappa < \Lambda$, otherwise the multifractality is only apparent at larger scales than the scattering.

(2) Simulating the clouds implies a finite number of realizations, which can be expressed quantitatively by the sampling dimension D_s (Schertzer and Lovejoy 1989) which is defined similar to the fractal dimension (eq. 2.1.1):

$$N_s \approx \lambda^{D_s} \tag{3.4.2}$$

For that reason being, there will be an almost surely maximum singularity γ_s^{\max} as well as an almost surely minimum singularity γ_s^{\min} present in the cloud sample. Note that the

latter does not always exist, but it does in the lognormal case. These two restrictions can easily be calculated by using the inverse cloud probability distribution exponent:

$$\gamma_s^{\min(\max)}(D_s) = c^{-1}(D + D_s) \quad 3.4.3$$

We recall that the free photon path length is $\tau_p = \kappa x = \kappa \lambda^{-1}$ and is dependent on λ . Consequently it is for our purpose necessary to consider $\gamma_s^{\min}, \gamma_s^{\max}$ as functions of λ . With the above relationship 2.5.5 and using the large κ approximation $\gamma_s \approx 0$ we obtain:

$$\gamma_p^{\min, \max}(\lambda) = 1 - \frac{1}{1 - \gamma_s(\lambda)} \quad 3.4.4$$

On the other hand:

$$\gamma_p(\lambda) = \frac{\log \tau_p}{\log \kappa} = 1 - \frac{\log \lambda}{\log \kappa} \quad 3.4.5$$

which derives simply from equation 2.5.1. We could now eliminate $\log(\lambda)$ and directly obtain the minimum/maximum order of photon singularity $\gamma_p^{\min, \max}$ in terms of the minimum/maximum order of cloud singularity $\gamma_s^{\min, \max}$ independent of the scale ratio λ . A graphical method is however clearer: We plot both curves (eq. 3.4.4. and eq. 3.4.5) versus $\log(\lambda)$ and obtain the range of validity for the order of photon singularity γ_p (see Fig. 3.7). We note that with increasing extinction coefficient κ , the maximum order of photon singularity γ_p^{\max} decreases and with increasing number of samples N_s or increasing codimension of the mean C_1 , the maximum order of photon singularity γ_p^{\max} increases as well.

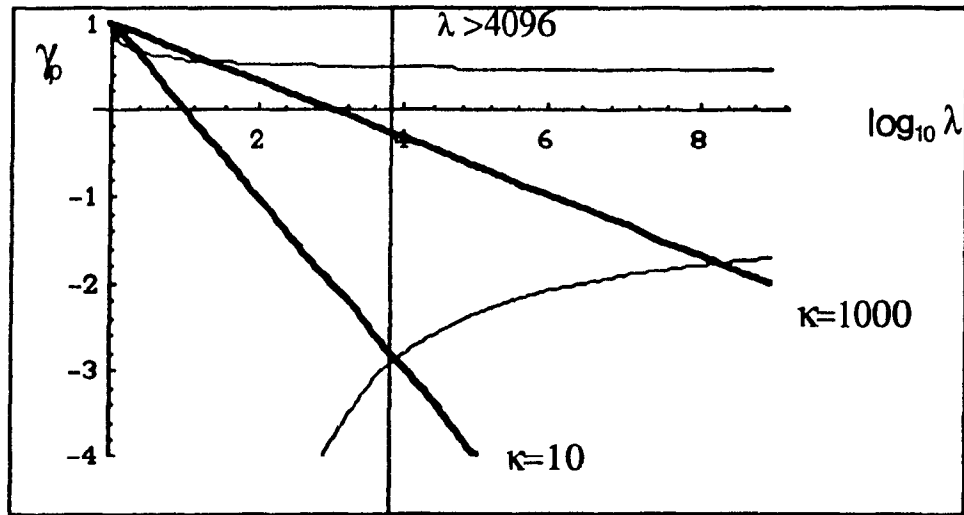


Figure 3.7: Range of validity for γ_p due to finite sample size and finite resolution. Depending on the extinction coefficient κ one can see different limits $\gamma_p^{\min}, \gamma_p^{\max}$ on γ_p which are shown by the intersection points. Note that each order of singularity γ_p represents one most probable distances in the cloud, as shown by the straight lines $\gamma_p(\lambda)$. The shaded region is not accessible since it represents scales (λ) smaller than the highest resolution Λ (here $\Lambda = 4096$).

As Figure 3.7 shows, the left branch of the dressed photon free path probability distribution exponent $c_{p,d}(\gamma_p)$ is in actual fact more strongly restricted by the resolution limit (1) than through the above restriction due to the sampling dimension of the cloud (2). More precisely the minimum order of photon singularity γ_p^{\min} due to the smallest size of resolution can be calculated as:

$$\gamma_p^{\min} = 1 - \frac{\log \Lambda}{\log \kappa} \quad 3.4.6$$

For example an extinction coefficient $\kappa=256$ and a scale of resolution $\Lambda^{-1} = 1/4096$ leads to the minimum order of photon singularity $\gamma_p^{\min} = -0.33$. This can be seen in Figure 3.3 and 3.5..

3.5 Moment Scaling Exponent

The further analysis consists in comparing the dressed moment scaling exponent $K_{p,d}(q)$ with the analytically bare moment scaling exponent $K_p(q)$ (eq. 2.5.9). Therefore we check the scaling of the moments of the dressed photon path length with respect to κ :

$$\langle \tau_p^q \rangle \approx \kappa^{K_{p,d}(q)} \quad 3.5.1$$

This is done by plotting $\log \langle \tau_p^q \rangle$ versus $\log \kappa$ (Figure 3.8; 3.10) after calculating the dressed moments:

$$\langle \tau_p^q \rangle = \sum_{i=1}^{\Lambda} \kappa^{-q} x_i^q \frac{\langle T(x_{i-1}) \rangle - \langle T(x_i) \rangle}{\Lambda^{-1}} \quad 3.5.2$$

where $\frac{\langle T(x_{i-1}) \rangle - \langle T(x_i) \rangle}{\Lambda^{-1}}$ is the discrete probability of the dimensionless photon path distance $\tau = \kappa x_i$ ($i=1, \dots, \Lambda$). If the dressed moments are scaling (i.e. they obey equation 3.5.1), the points for each specific moment q lie on a straight line, whose slope is $K_{p,d}(q)$ (Figure 3.8; 3.10). We then compare we the "dressed" moment scaling exponent $K_{p,d}(q)$ with the analytically derived $K_p(q)$ in Figure 3.9 and 3.11.

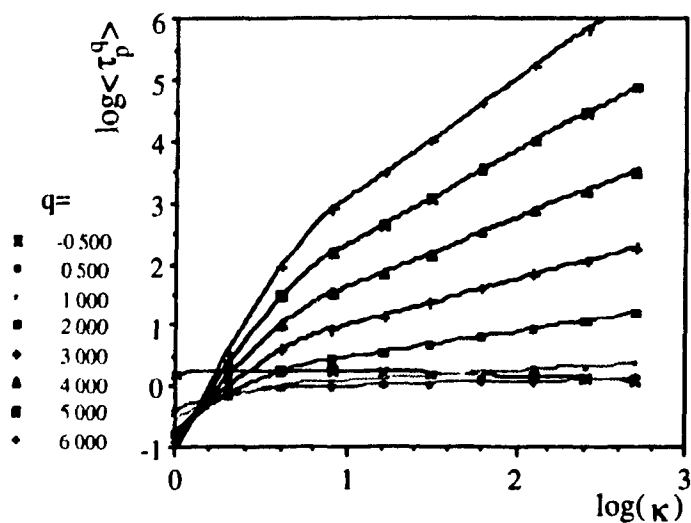


Figure 3.8: Scaling of the moments of the dressed photon path length τ_p as a function of κ . $\log_{10} \langle \tau_p^q \rangle$ versus $\log_{10}(\kappa)$ for various values of q . There is a very good scaling for $\kappa > 8$ since the lines are straight in that regime. The scaling breaks down for smaller κ since a unique normalization is not provided anymore. Data from simulation with $\alpha=2$, $C_1=0.1$, 4096 realizations, 512 photons/realization

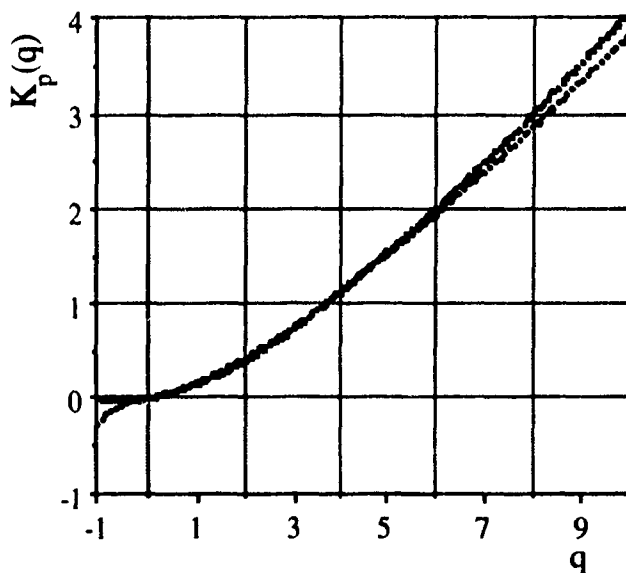


Figure 3.9: Comparison of the moment scaling exponent function $K_p(q)$ for the "bare" with $K_{p,d}(q)$ for the "dressed" photon path length for a field $\alpha=2$, $C_1=0.1$. In the range $-0.5 < q < 6$ both curves are in very good agreement. The dressed $K_{p,d}(q)$ curve was obtained from the simulation with 4096 realizations, 512 photons/realization.

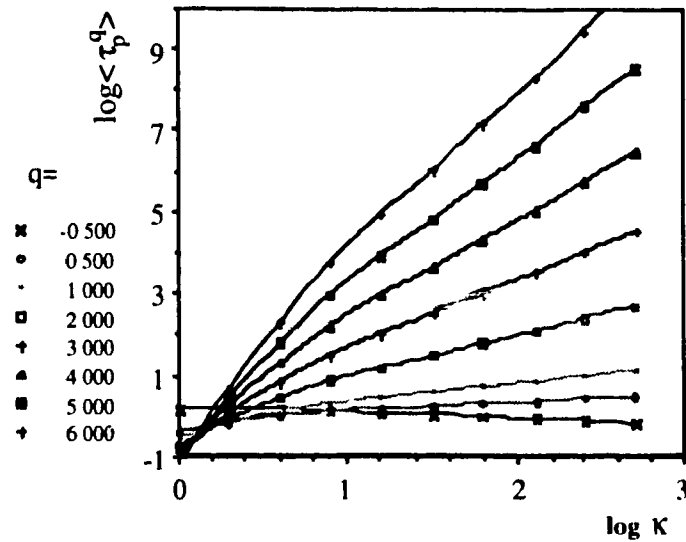


Figure 3.10: Scaling of the moments of the dressed photon path length τ_p as a function of κ . $\log_{10} \langle \tau_p^q \rangle$ versus $\log_{10}(\kappa)$ for various values of q . There is a very good scaling for $\kappa > 8$ since the lines are straight in that regime. The scaling breaks down for smaller κ since a unique normalization is not provided anymore. Data from simulation with $\alpha=2$, $C_1=0.5$ 4096 realizations, 512 photons/realization and the scaling regime ($8 < \kappa < 512$).

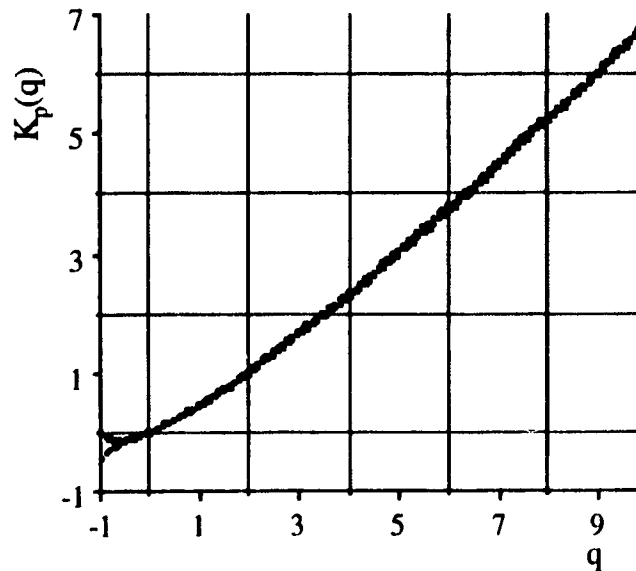


Figure 3.11: Comparison of the moment scaling exponent function $K_p(q)$ for the "bare" with $K_{p,d}(q)$ for the "dressed" photon path length for a field $\alpha=2$, $C_1=0.5$. In the range $-0.5 < q < 10$ both curves are in very good agreement. The dressed $K_{p,d}(q_p)$ curve was obtained from the simulation with 4096 realizations, 512 photons/realization and the scaling regime ($8 < \kappa < 512$).

3.6 Limits of Validity for the Moment Scaling Exponent

The range of validity for the numerical simulation of the moment scaling exponent $K_p(q)$ arises out of the same restrictions as for the photon singularities γ_p . The moment scaling exponent $K_p(q)$ is related to the probability distribution exponent $c_p(\gamma_p)$ by the Legendre Transformation of 2.2.3. The order of moments are the derivatives of the probability distribution exponent (eq. 2.2.4):

$$q = c_p'(\gamma_p) = \frac{1-(1+C_1)^2(1-\gamma_p)^2}{4C_1(1-\gamma_p)^2} \quad 3.6.1$$

thus the restrictions for the dressed moments simply are the slopes of the photon free path probability distribution exponent at its minimum/maximum order of photon singularities $\gamma_p^{\min}, \gamma_p^{\max}$. This yields for example $q^{\min} = c_p'(-0.33) = -0.8$ and $q^{\max} = c_p'(0.8) = 10.4$ in the case $C_1=0.5$.

The moments for which there is a good agreement between the two moment scaling functions $K_p(q)$, $K_{p,d}(q)$ (Fig. 3.9; 3.11) represent photon distances which are the most probable ones, since this range of order of moments q corresponds to very low photon probability distribution exponents $c_p(\gamma_p)$ which on the other hand means high probabilities. It is obvious for $q=1$, since this moment is simply the expectation value of the free photon path (i.e. mean free path). In other words, the range of agreement belongs to distances which have the most significant contribution to the transmittance (see the next section).

4. Renormalization

We can now relate the transmission statistics of lognormal multifractal clouds to those of a homogeneous cloud. At first sight this seems to be a difficult task since we already explained in the introduction that in the thick limit (κ large) both types of clouds will result in a completely different behavior of the radiative transfer properties. In this chapter however we will show that the photon statistics of a multifractal cloud can be approximated by the photon statistics of a "renormalized" homogeneous cloud in a certain range of photon singularities. We will relate this to multiple scattering and to results of diffusion on multifractals.

4.1 Direct Transmission

We seek to replace the multifractal cloud with a nearly equivalent homogeneous cloud with "effective" extinction coefficient κ_{eff} . This cloud has the direct transmission given by $T(x) = e^{-\kappa_{\text{eff}}x}$. The moments of the nondimensional path length $\tau_p = \kappa x$ are then given by:

$$\langle \tau_p^q \rangle = \int_0^1 (\kappa x)^q p(x) dx \quad 4.1.1$$

with $p(x) = -\frac{dT}{dx} = \kappa_{\text{eff}} e^{-\kappa_{\text{eff}}x}$. In the limit of large κ_{eff} we obtain

$$\langle \tau_p^q \rangle \approx \left(\frac{\kappa}{\kappa_{\text{eff}}} \right)^q \Gamma(q+1) \quad 4.1.2$$

If we express κ_{eff} as a power of κ i.e. $\kappa_{\text{eff}} = \kappa^a$ above equation can be written as

$$\langle \tau_p^q \rangle \approx q \Gamma(q) \kappa^{q-aq} \quad 4.1.3$$

i.e. a homogeneous cloud has a linear exponent: $K_{p,\text{hom}}(q) = q - aq$. A linear $K_p(q)$ indicates exponential transmission $T(x)$ (note that the Legendre transformation breaks down in this case so that there is no corresponding $c_p(\gamma_p)$). Now we compare this with the $K_p(q)$ for a lognormal multifractal cloud. The corresponding value of a will actually be a slowly varying function of q , (as demonstrated in the Fig. 4.1)

$$a_m(q) = \frac{q - K_p(q)}{q} \quad 4.1.4$$

which for small q can be approximated by $a_m \approx a_m(0) = \frac{1}{1+C_1}$. To determine the optimum value of q , to use for this approximation, we write $\langle T \rangle$ in terms of $q=c_p'(\gamma_p)$ which indicates which q contributes to different transmittances (Fig. 4.3). The maximum transmittance occurs for $q=0$; this justifies our use of $q=0$ in the above. The maximum deviation of $a_m(q)$ from $a_m(0)$ for $-0.5 < q < 1$ lies between 10% to 15% for $0.1 \leq C_1 \leq 0.9$ respectively (Fig. 4.1). The linear approximation $K_p(q) \approx q - qa_m(0)$ leads to a renormalized extinction coefficient of the homogeneous cloud:

$$\kappa_{eff} = \kappa^{1/C_1} \quad 4.1.5$$

The linearity of the $K_p(q)$ function, and hence accuracy of the approximation in the range $q \approx 0 - 3$ can be seen in Figure 3.9; 3.11.

Figure 4.2 compares the direct transmission of a "renormalized" homogeneous cloud with the transmission through a bare multifractal cloud and the transmission through a dressed multifractal cloud.

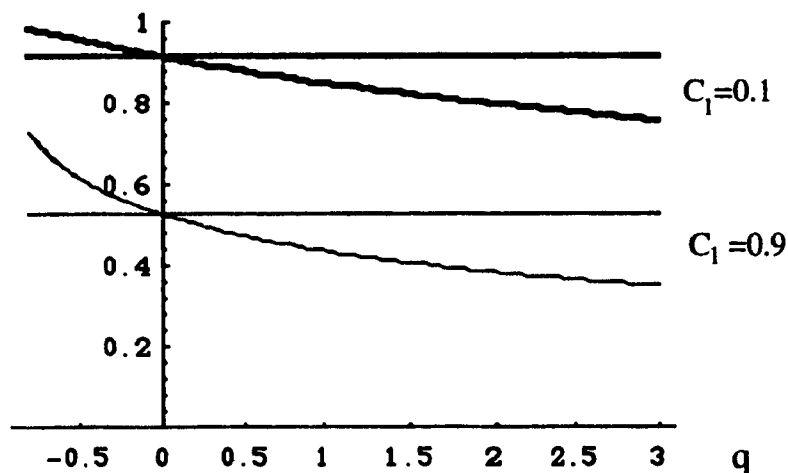


Figure 4.1: The effective scaling exponent $a = s/q = \left(\sqrt{(1+C_1)^2 + 4C_1q} - (1+C_1) \right) / (2C_1q)$ is slowly varying function which departs from the approximation $a = (1+C_1)^{-1}$ for $-0.5 \leq q \leq 1$ by less than 9% for $C_1=0.1$ (thick lines) and less than 15% for $C_1=0.9$.

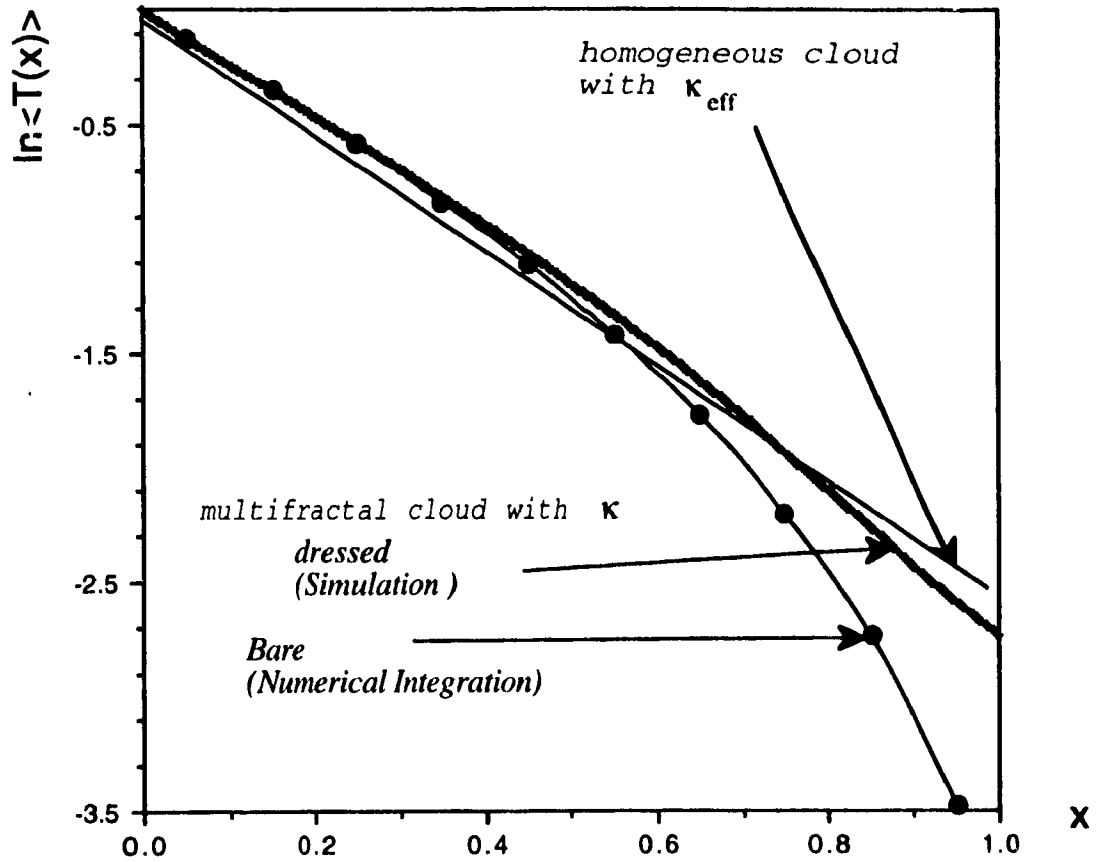


Figure 4.2: Transmission through a multifractal cloud $C_1=0.5$ (bare and dressed case) with $\kappa=4$ compared to the transmission through a homogeneous cloud with the "renormalized" extinction coefficient $\kappa_{eff} = \kappa^{1/C_1} = 2.52$. Note the natural logarithmic scale $\ln_e\langle T(x)\rangle$.

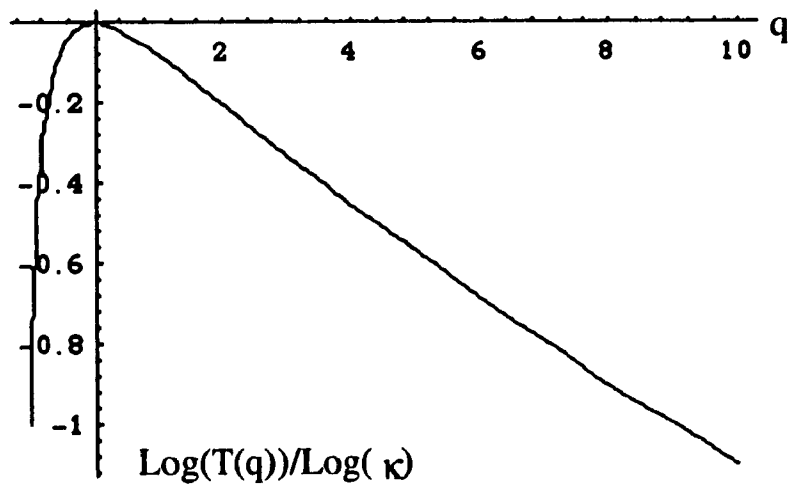


Figure 4.3: Transmission as a function of the moments $T(q)/\log_{10}(\kappa)$

4.2 Some Considerations on Multiple Scattering

We have seen that for direct transmittance, the near linearity of $K_p(q)$ leads to the possibility of "renormalizing" the multifractal: it is nearly equivalent to a homogeneous medium with an effective extinction coefficient $\kappa_{eff} \approx \kappa^a$. This suggests that by using this approximation we can extend our previous treatment beyond direct transmission to take into account multiple scattering and obtain an approximation for the overall transmittance and reflectance of a lognormal multifractal cloud. The main issue herein is the near linearity of $K_p(q)$ which means that the correlations between consecutive free photon paths are almost insignificant.

A detailed study of this will be published elsewhere. Here we test this idea by considering the numerical transmission results on lognormal multifractal clouds (with $C_1=0.5$) published in Davis et al 1991, 1993 (see Fig. 4.4). These simulations were made using two dimensional discrete lognormal cascades with scale ratio factor 2 per step, total range of scales 2^{10} . Cyclic boundary conditions were used in the horizontal and photons were vertically incident. Isotropic discrete angle phase functions were used and the resulting fields in each of the four directions at 90° , as well as the overall albedo and transmission were calculated by both Monte Carlo and relaxation techniques (the agreement of the two methods increased confidence in the results). The extinction coefficient was increased by factors of two so that the total mean optical depth $\kappa \langle |\bar{x}| \rangle$ increased from 12.5 to 200.

With the goal to obtain a theoretically predicted renormalization result, we recall that for plane parallel clouds, with the same boundary conditions and the "Discrete Angle (2,4)" radiative transfer phase functions (Lovejoy et al 1990), $T = \frac{1}{1 + \frac{1}{2}(1-t+r)\tau}$ where t and r are the discrete angle forward and backward scattering coefficients respectively. In Davis et al 1991 isotropic "Discrete Angle" phase functions were used (i.e. $t=r=1/2$). Using this result and the effective extinction coefficient in place of the true optical depth $\tau = \kappa_{eff} \langle \rho \rangle = \kappa_{eff}$, we obtain:

$$\langle T \rangle = \frac{1}{1 + \frac{1}{2} \kappa_{eff}^{-1+C_1}} \approx 2 \kappa_{eff}^{-\frac{1}{1+C_1}} \quad 4.2.1$$

Fig. 4.4 shows the result of superposing this function on Davis et al's results, which are nearly power law even for κ as low as 12.5. The total transmittances through the renormalized homogeneous cloud show for all values of κ only less than 20% difference from the total transmittances through the multifractal cloud. The actual (multiple scattering) result is slightly higher than the renormalization prediction, which is

expected since $a(q) \leq \frac{1}{1+C_1}$ for all values of $q > 0$ (negative values of q correspond to very small path lengths, which contribute only insignificantly to the total transmittance). Therefore the approximation leads to a slightly lower direct transmission, resulting also in a lower total transmission. Closer examination shows that there is a slight curvature suggesting that there are still some residual small κ effects and that a better estimate might be obtained by considering only his last two points. Indeed, this is remarkably close to the theoretical renormalization result ($a=2/3$) since it yields $a \approx 0.65$. These results suggest that renormalization will give accurate results for bulk transport properties in multifractal systems with other boundary conditions, even with modest optical thicknesses.

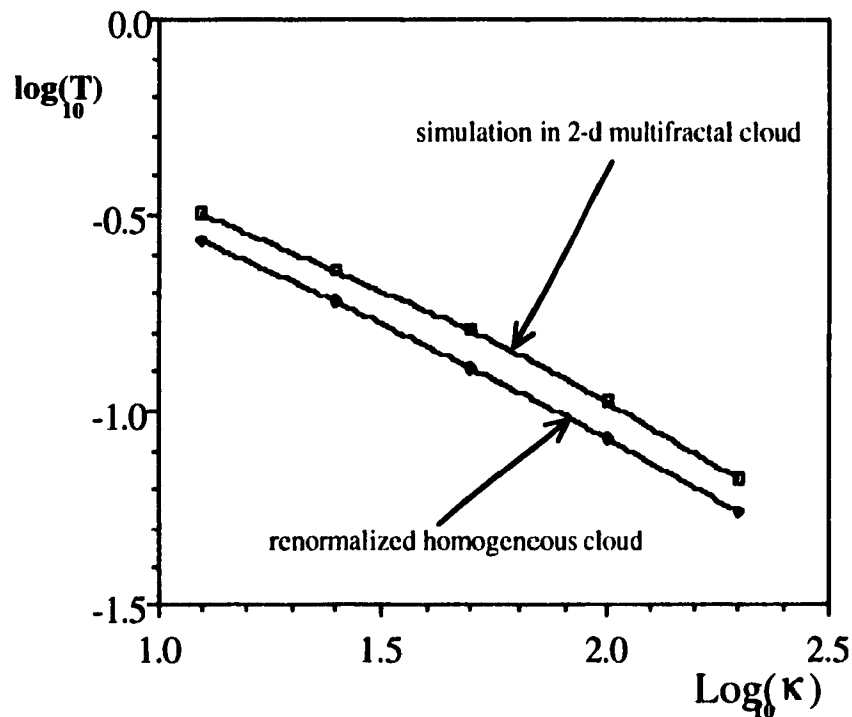


Figure 4.4: Result on total transmission after multiple scattering through 2-d multifractal cloud ($C_1 \approx 0.5$), published in Davis et al 1991, compared to the thick cloud limit of the transmission through a homogeneous cloud with renormalized extinction coefficient κ_{eff} .

4.3 Comparison with Diffusion

The surprisingly accurate prediction of the Davis et al 1991 thick cloud numerics can perhaps best be understood by considering the relation between radiative transfer and diffusion in multifractals. In general, there will be two significant limits; the large Λ (wide cascade range) and large extinction coefficient κ (thick cloud) limits. Clearly, for fixed and finite Λ , if the cloud is made thick enough, ($\kappa \gg \Lambda$) the mean free path will be much smaller than a single resolution element and the photons will diffuse through each homogeneous region of size Λ^{-1} (see section 3.4b (1)). The overall result will be photons diffusing through the multifractal cloud. In actual fact, diffusion can still occur under somewhat less stringent conditions when κ is large, the main requirement being that weak density regions become so rare that direct photon transmittance across a large fraction of the cloud is statistically negligible. The multifractals with $\alpha < 2$ have precisely the property that they are dominated by weak events (negative singularities) called "Levy holes". It is a priori possible that, even with large κ , if Λ is sufficiently large (the order of the limits $\Lambda \rightarrow \infty$ and $\kappa \rightarrow \infty$ is important i.e. with κ fixed, but with $\Lambda \rightarrow \infty$) they will have large regions dominated by the holes, and hence lead to nondiffusive transfer.

However, in the case studied here, the parabolic shape of the cloud probability distribution exponent $c(\gamma)$ (eq. 2.2.6a) guarantees that large negative orders of moments γ and the corresponding weak regions are extremely rare, indeed, in the preceding development, we have seen that the value of κ is essentially irrelevant as long as it is sufficiently large. We therefore anticipate that the photons will diffuse for large enough κ . To make this plausible, we cite a recent analytic result believed to be exact for diffusion in one dimensional multifractals with existing moment scaling exponent $K(-1)$ (Silas 1994):

$$\langle l^2 \rangle \propto t^{\frac{2}{2+K(-1)}} \quad 4.3.1$$

which yields in the lognormal multifractal case:

$$\langle l^2 \rangle \propto t^{\frac{1}{1+C_1}} \quad 4.3.2$$

for the RMS particle distance l after time t in a lognormal multifractal with codimension of the mean equal to C_1 . Since $(\kappa_{\text{dim}} \langle \rho_{\text{dim}} \rangle)^{-1}$ is a typical diffusive distance per diffusion step, for normal diffusion, we can write the nondimensional diffusion result:

$$\frac{\langle l^2 \rangle}{(\kappa_{\text{dim}} \langle \rho_{\text{dim}} \rangle)^{-2}} = \frac{\langle x^{-2} \rangle}{\kappa^{-2}} \approx N \propto \frac{t}{\tau} \quad 4.3.3$$

where N is the number of steps and τ is the time per step). In the multifractal medium, the particle “slows down”. However, the typical step can be used to define the effective κ as κ_{eff}^{-1} and dimensional analysis combined with the anomalous diffusion result now yields:

$$\left(\frac{\langle x^2 \rangle}{\kappa_{\text{eff}}^{-2}} \right)^{1+C_1} \propto \frac{t}{\tau} \quad 4.3.4$$

hence comparing this with the above result for normal diffusion, we obtain:

$$\kappa_{\text{eff}} \propto \kappa^{1+C_1} \quad 4.3.5$$

The above multiple scattering idea is therefore completely consistent with the diffusion results. Note that for diffusion in spaces with dimensions higher than one, the above diffusion result is no longer exact, whereas our scattering arguments will be valid (to varying degrees of approximation) in a space of any dimension.

5. Analysis of empirical cloud data

In this chapter we analyze the liquid-water-content (LWC) of stratocumulus cloud data to experimentally test the validity of the universal multifractal cloud model. This study establishes the first investigation of the universal multifractal indices of cloud liquid-water-content. We show that the examined clouds are very well scaling over the whole examined range (5m-330km) and can be described by lognormal universal multifractals. As mentioned in section 2.2, universal multifractals are classified by three parameters (H , C_1 , α) which we determine.

5.1 The Cloud Liquid Water Data

The LWC-data was obtained from the FIRE (First ISCCP [International Satellite Cloud Climatology Project] Regional Experiment) in June/July 1987 off the coast of California (Albrecht et al. 1988). This project took place in order to study the extensive fields of stratocumulus clouds that are a persistent feature of subtropical marine boundary layers. Marine stratocumulus clouds are important components of the Earth's climate system since they significantly enhance the albedo over large areas of oceans. For example, Randall et al. 1984 estimated that a four percent increase in the area covered by these clouds could balance the warming that might be expected from a doubling of CO_2 . This is an important reason for general-circulation models (GCMs), that are used for climate studies, to simulate realistically the distribution of marine stratocumulus clouds. Observations such as those collected during the ISCCP clearly show major discrepancies between the simulated and observed distribution of stratocumulus cloudiness.

The LWC measurements were taken with a King hot wire probe at a frequency of 20 Hz mounted on an aircraft flying with a speed of roughly 100 m/s. The principle of operation of the sensor is the measurement of the power required to maintain the temperature of a hot wire on which cloud droplets are impacting. The sensitivity (i.e. minimum detectable concentration) was 0.02 g/m^3 and the wire had a response time of less than $1/30 \text{ s}$. The accuracy was 5% at 1 g/m^3 . For further instrumental details see King et al 1980. Using the aircraft speed, the time series can be converted into distances, i.e. the spatial resolution is about 5m.

The data set analyzed here is from different aircraft runs, the smallest containing 8192 points (corresponding to a range of scales 5m-41km), with the largest containing 65536 points (corresponding to a range of scales 5m-328km). Figure 5.1 shows a typical fragment of the data. In Figures 5.2a,b we show the histogram of the raw data. The

most probable density was $\rho \approx 0.32 \text{ g/m}^3$. It is interesting to note, that there are very few data points with a density below 0.05 g/m^3 .

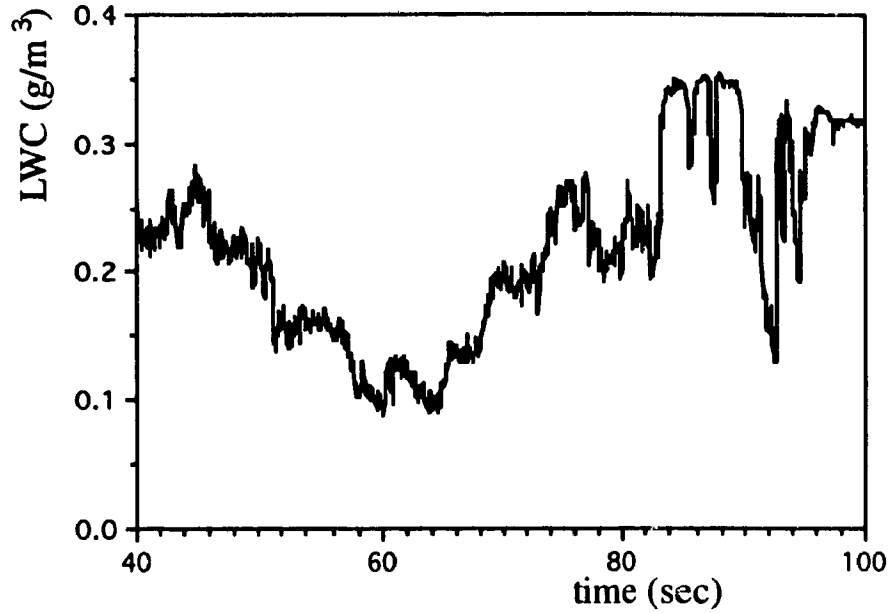


Figure 5.1: A typical fragment of the cloud LWC- data. Fragment from data set #4.

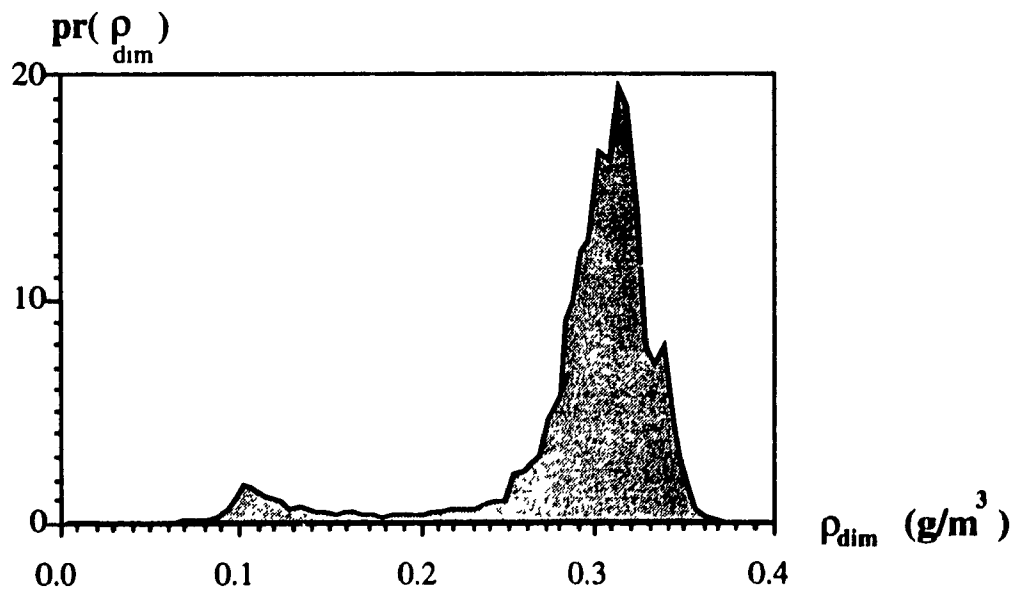


Figure 5.2a: Histogram of the raw LWC-data

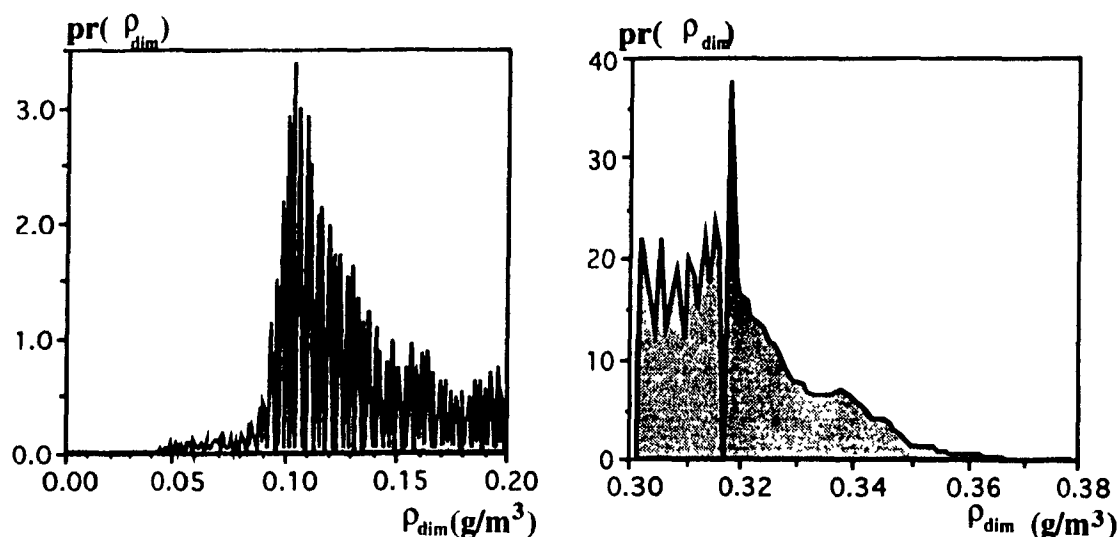


Figure 5.2b: Histogram for the low and high values (zoom of 5.2a)

5.2 Power spectrum

Looking at the 1-D power spectrum (the squares of the moduli of the Fourier components of the LWC-data, i.e. $|\hat{\rho}_k|^2$) one can gain direct information about scaling (power law behavior under changes in spatial resolution). Figure 5.3 shows that all five LWC data sets are scaling over the whole range, corresponding to a range of spatial scales from 5m-330km. The absolute slopes for each data set, obtained by linear regression, are listed in table 5.1.

Number of data set	Date	Time	Number of points	Absolute Slopes in power spectrum = β
1	30.6	-	26632	1.59
2	2.7	-	16384	1.54
3	14.7	-	65536	1.65
4	16.7	17:17	8192	1.70
5	16.7	18:19	12028	1.45

Table 5.1: Size and absolute spectral slope of the LWC-data sets.

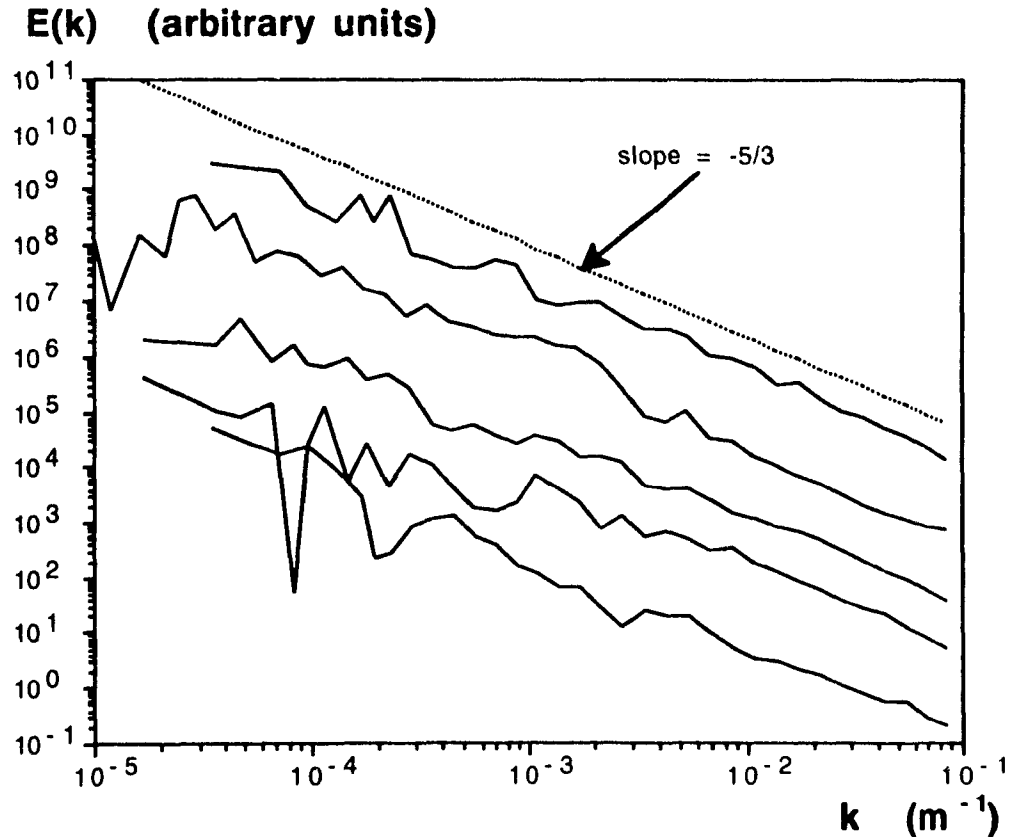


Figure 5.3: Power spectrum of the 5 different data sets (averaged to 10 points per magnitude on the k -axis). All the sets are very accurately scaling and have absolute slopes close to the value of the standard turbulence theory $\beta = 5/3$ (straight line on top of graph). In order to avoid overlap, the lines were offset vertically by an order of magnitude each. Number of sets used to compute the average from top to bottom: 4, 3, 1, 2, 5.

If cloud droplets were passive scalars, i.e. transported by the wind without interacting with it, and if we neglect intermittency corrections, one obtains the standard turbulence theory (Obhukhov 1949, Corrsin 1951). The theoretical value for the spectral slope of the process is $\beta_{\text{theo}} = 5/3$. The so called Corrsin-Obhukhov law for passive scalars is:

$$E(k) \approx k^{-\frac{5}{3}} \quad 5.2.1$$

where k is the wave number. The values from the empirical data (Figure 5.3) obtained by linear regression are in a range of ± 0.2 around this theoretical value (Table 5.1).

Since the power spectrum shows roughly the same slope for all 5 data sets the original data can be split up into 15 pieces, each containing 8192 points. We assume that

these data sets of equal size are statistically independent and therefore the numbers of samples is $N_s=15$. In the following the ensemble average refers to averaging over these 15 data sets. An ensemble averaged power spectrum (the ensemble average is taken over the squares of the moduli of the Fourier components, $|\hat{\rho}_k|^2$) yields $\beta \approx 1.70$, slightly higher than the passive scalar value in standard turbulence theory. Figure 5.4 shows that also here very accurately scaling is obtained.

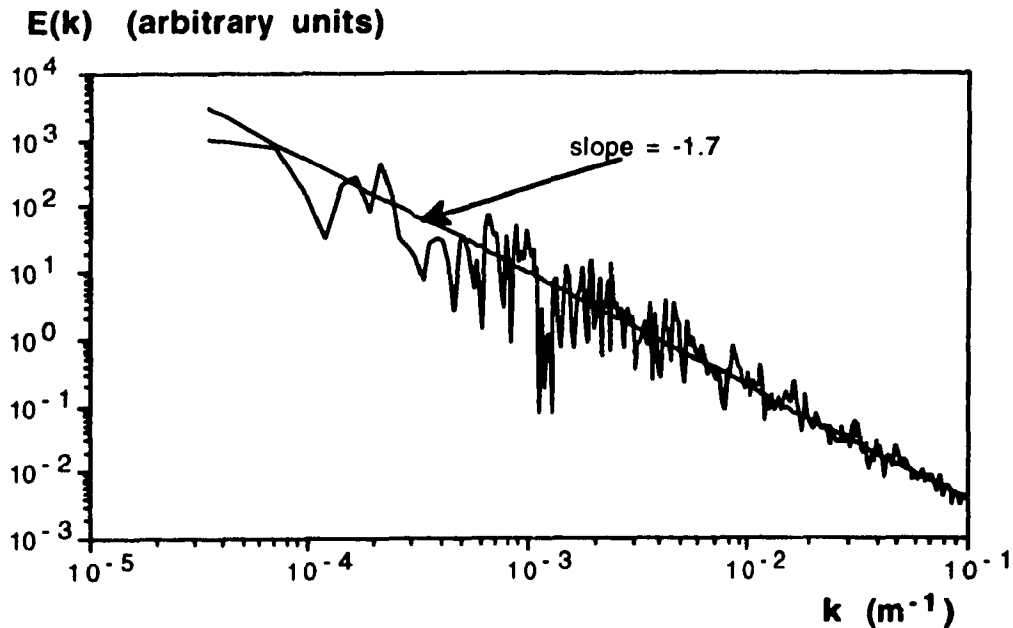


Figure 5.4: Ensemble averaged power spectrum (averaged to 100 points per magnitude on the k axis). The ensemble average of the squared moduli of the 15 equal sized data sets yields a power spectrum with a spectral slope $\beta=1.7$

A particularly impressive example of the scaling is given in Fig. 5.3, the power spectrum of the longest data set #3 (65536 points i.e., spanning the range of scales of 5m-330 km) which is scaling throughout the entire range. Recall that scaling is a statistical symmetry; hence it is broken on every single realization, the random fluctuations in the spectrum are expected. It is plotted with a higher resolution (averaged to 100 points per magnitude) in a separate graph (Figure 5.5). The standard model of atmospheric dynamics (e.g. Monin 1972) divides the atmosphere into two fundamentally distinct regimes which are scaling: a small scale three-dimensional turbulent regime and a large scale two-dimensional turbulent regime. Unlike turbulence in three dimensions, in two dimensions, vortex stretching is inhibited and vorticity is conserved. This leads to quantitatively distinct two-dimensional and three-dimensional behavior: the standard

model assumes that these different regimes are separated by a "mesoscale gap" whose scale is expected to be of the order of the height of the atmosphere (approximately 10km). This existence of the "gap" has been periodically questioned on empirical grounds since the late 1960's, and due to the remarkable progress in scaling ideas in recent years, it also seems out-dated from a theoretical point of view (Tessier et. al. 1993a). The power spectrum below gives strong credence to these doubts. It not only shows clear evidence of scaling right through the crucial mesoscale, it is also the example of scaling covering the widest range that we are aware of in the atmosphere (for a single data set).

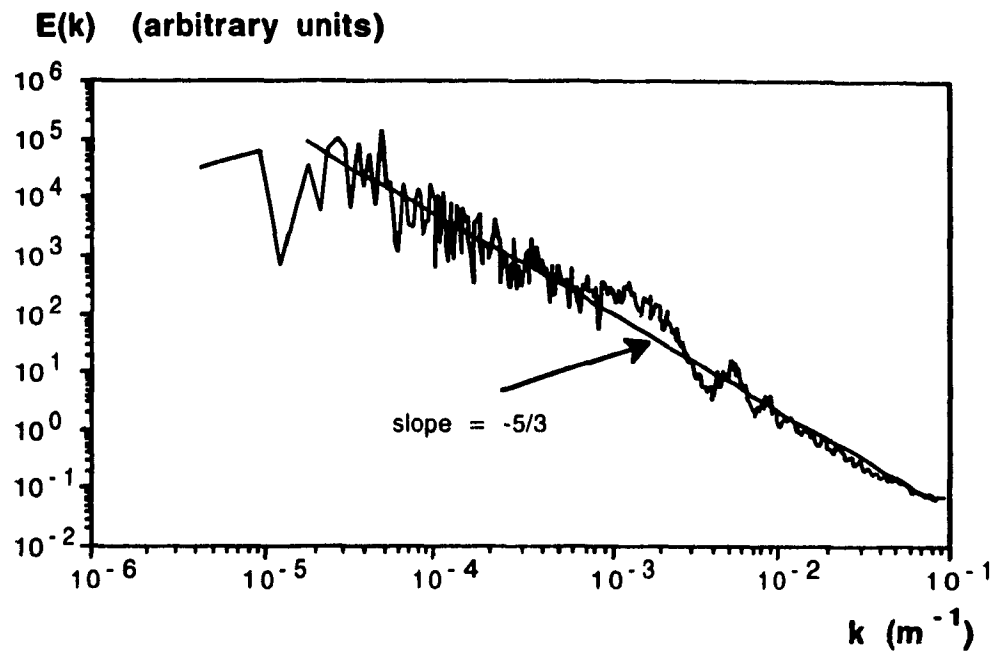


Figure 5.5: Power spectrum of data set number 3 (65536 points) (averaged to 100 points per magnitude on the k axis). The spectrum is excellent scaling with the spectral slope $\beta \approx 5/3$ in the whole range 5m-330km.

5.3 Structure function

The structure function $\zeta(q)$ is a scaling exponent from which we can retrieve universal multifractal indices H and C_1 . It has the following definition:

$$\langle |\Delta\rho|_\lambda^q \rangle \approx l^{\zeta(q)} \quad 5.3.1$$

where $l=\lambda^{-1}$ is the small scale and the largest scale is assumed to be equal to one. Notice that by keeping the sign of the increment, the "structure" of the recursively coarsened signal is retained. The structure function is related to $K(q)$ and H in the following way:

$$\lambda^{-\zeta(q)} \approx \langle |\Delta\rho|_\lambda^q \rangle \approx \langle \varphi_\lambda^{qa} \rangle \lambda^{-qH} \approx \lambda^{K(qa)-qH} \quad 5.3.2$$

which we obtain with equation 5.4.2 below and by substituting x by λ . Note φ_λ is the conserved property of the process, $\langle \varphi_\lambda \rangle = \text{constant}$ (independent of scale) and here a is equal to one (see paragraph 5.4 for a detailed explanation). Equation 5.3.2 relates the structure function with the moment scaling exponent:

$$\zeta(q) = qH - K(q) \quad 5.3.3$$

Therefore for $q=1$ the structure function yields the parameters:

$$H = \zeta(1) \quad 5.3.4$$

$$C_1 = \zeta(1) - \zeta'(1) \quad 5.3.5$$

which is retrieved by using the basic properties of the moment scaling exponent $K(1)=0$ and $K'(1)=C_1$ (equation 2.2.5b).

The empirical structure function is obtained by a procedure known from the previously estimated moment scaling exponent (section 3.5). At first the logarithm of the moment $\log_{10} \langle |\Delta\rho|_\lambda^q \rangle$ is plotted versus $\log_{10}(\lambda)$ keeping q fixed (Fig. 5.6). The lines show fair scaling in the range $1.2 < \log(\lambda) < 3.0$. The slopes of a least mean square fit in that range yields the empirical estimate of $\zeta(q)$ (Fig. 5.7). The structure function at q equal to one gives $\zeta(1)=0.29$ and $\zeta'(1)=0.20$. Therefore the degree of stationarity of the observed field is $H=0.29$, which is little below the passive scalar value of $1/3$ (see next section). The codimension of the mean is estimated as $C_1=0.09$.

Note that for values of q larger than a critical value $q \approx 2.3$ the structure function becomes linear with a slope around 0.06 (Fig. 5.7). This indicates a phase transition for values of q larger than a critical value $q \approx 2.3$. A priori, it could be a second order phase transition due to sampling limitations (q_s), or a first order phase transition corresponding to divergence of the moments (q_D); however in section 5.6 below we argue that it is more likely to be of first order.

Davis et al 1994 calculated the power spectrum, the structure function and the moment scaling exponent $K(q)$ of the absolute differences for a single realization (8192 data points) of the FIRE 87 data. Their estimates were $H=0.28$, $C_1 \approx 0.1$ and $\beta=1.4$. Although we expect large sample to sample variations so that estimates based on one single sample are not sufficient, their results are surprisingly close to the ones we estimated. Particular large sample to sample variations are expected for the estimate of β , as seen in the previous section, so that their estimate of β is not very promising.

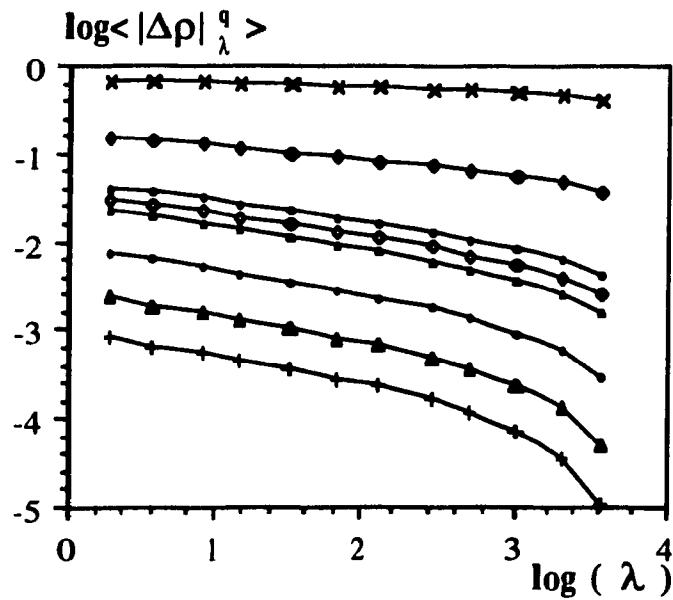


Figure 5.6: Scaling of the gradients of the raw LWC-data. The graph shows $\log_{10}\langle |\Delta\rho|_{\lambda}^q \rangle$ versus $\log_{10}(\lambda)$. In the range of $0.6 < \log_{10}(\lambda) < 3.0$ the scaling is respected. A linear regression in that regime yields the structure function $\zeta(q)$ (see below). Following moments were plotted (q from top to bottom): 0.1, 0.5, 0.9, 1.0, 1.1, 1.5, 2.0, 2.5. Note the break in scales for large λ , particularly for q larger than the critical $q \approx 2.3$. Moments of the order larger than this critical value will not converge anymore, thus the statistics will be poor.

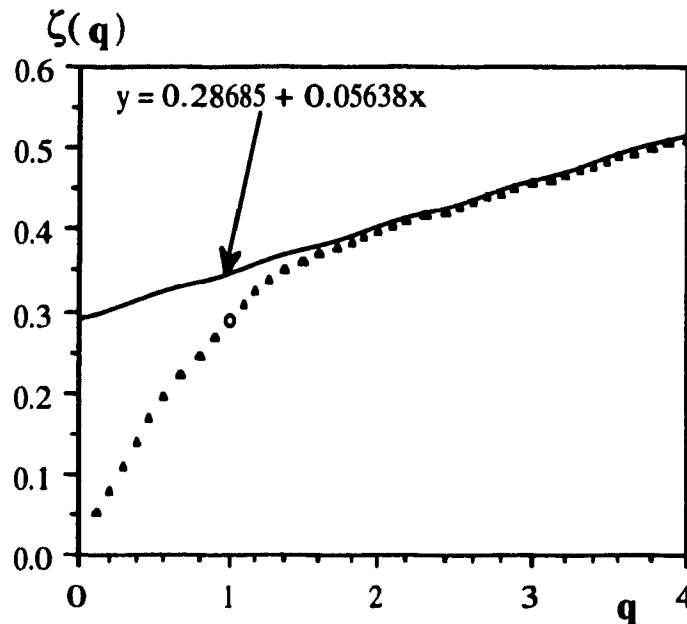


Figure 5.7: Structure function $\zeta(q)$ versus q . From $\zeta(1)$ and $\zeta'(1)$ one yields the universal multifractal indices $H=0.29$ and $C_1=0.09$. Note that for values of q larger than a critical value $q=2.3$ the structure function becomes linear corresponding to a multifractal phase transition.

5.4 Transformation of the Data into a Conserved Multifractal

Most analysis techniques used in the further analysis are sensitive to unconserved multifractal fields (i.e. $H \neq 0$). Therefore, in the first step the parameter H of our data is estimated.

In real space the equivalent equation to Corrsin-Obhukhov law (eq. 5.2.1) is:

$$\langle |\Delta \rho(x)| \rangle \approx x^{\frac{1}{3}} \quad 5.4.1$$

Statistically, this means that the characteristic fluctuations $\Delta \rho$ are scale invariant with respect to λ (using our notation: $\lambda = x^{-1}$). That is, the fields are not conserved and $H = 1/3$. We may write the passive scalar scaling for the density ρ as:

$$|\Delta \rho_\lambda| \approx \varphi_\lambda^a \lambda^{-H} \quad 5.4.2$$

where φ_λ has the conserved property $\langle \varphi_\lambda \rangle = \text{constant}$ (independent of scale). Since we have as yet no proper dynamical theory for the liquid-water distribution in the atmosphere, we do not know the appropriate fields φ_λ nor the corresponding value of a . In the following discussion, therefore, the simplifying assumption is made that $a=1$ (changing the value of a corresponds essentially to changing the parameter C_1 , see eq. 5.5.5b). H has a straightforward interpretation: it specifies how far the measured field ρ is from the conserved field φ : $\langle |\Delta \rho| \rangle \approx \lambda^{-H}$. In other words, power-law filtering (also called fractional differentiating) of the measured field ρ leads to the conserved field φ .

Fractional differentiating can be considered as a generalization of the usual differentiation by a non-integer order. A differentiation of the integer order n can be performed in Fourier space by multiplying the Fourier components by a factor of k^n . The same operation for a non-integer order H is called fractional differentiation (or for $H < 0$ fractional integration). In practice we multiply the Fourier components of the data $\hat{\rho}_k$ by $|k|^{\frac{1}{3}}$. Since we differentiate, the mean is equal to zero, which is achieved by setting the 0th Fourier component $\hat{\rho}_0 = 0$. After fast-Fourier transforming the data back into physical space, the absolute value of the data is taken.

Figure 5.8 shows a fragment of the LWC-data after fractional integration. Since it is the same fraction as shown in Figure 5.1 the effect of power law filtering can be clearly seen. Singularities present in the field are accentuated, the field is rougher due to the relative boosting of the high frequencies.

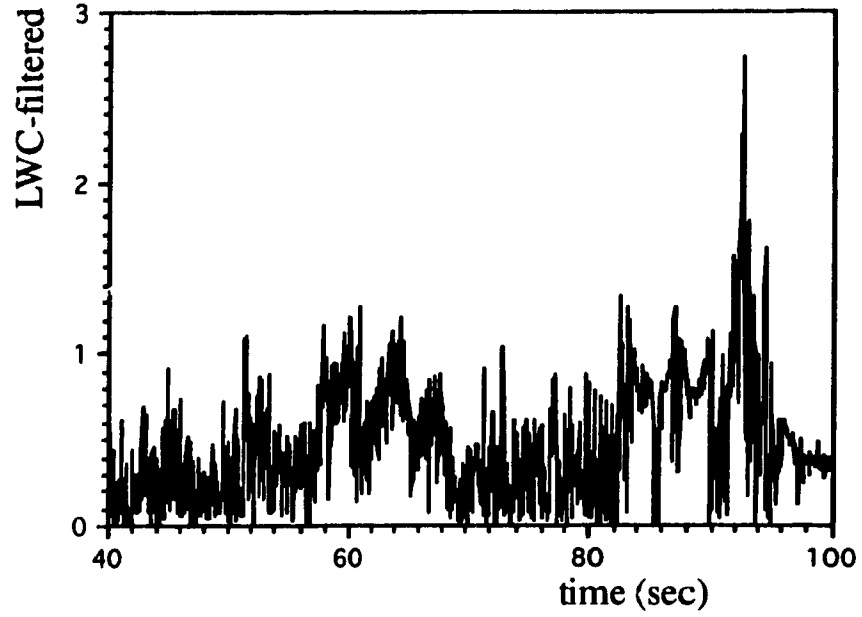


Figure 5.8 LWC-data after fractional differentiation by a factor of $H=1/3$. Same fragment from data set #4 as in Figure 5.1.

5.5 Double Trace Moment Analysis

The Double Trace Moment Technique is a powerful technique designed to directly determine the universal multifractal indices α and C_1 (Lavallée 1991, Lavallée et al. 1992). The basic idea of the DTM-technique is to directly exploit universality by generalizing the trace moment. It introduces a second moment η by transforming the field at the scale of resolution Λ : $\varphi_\Lambda \rightarrow \varphi_\Lambda^\eta$. The scaling behavior of this field is then studied by looking at the various q th moments at increasing scales λ (remember $\lambda < \Lambda$). The obtained q, η double trace moment at resolution λ and Λ has the following scaling behavior:

$$Tr_\lambda (\varphi_\Lambda^\eta)^q = \left\langle \sum_{A_\lambda} \left(\int_{A_\lambda} \varphi_\Lambda^\eta dx^D \right)^q \right\rangle = \lambda^{K(q,\eta)-(q-1)D} \quad 5.5.1$$

where A_λ is the set A at resolution λ and D is the dimension of the embedding space (here $D=1$). The integration over A_λ rescales the field and dresses the quantities. The sum is over all the A_λ sets. When $\eta=1$ the right hand side of eq. 5.5.1 reduces to the usual trace moment. The above double scaling exponent $K(q,\eta)$ is related to the moment scaling exponent $K(q)$ (see section 2.2) by the following relation:

$$K(q, \eta) = K(q\eta) - qK(\eta) \quad 5.5.2$$

$K(q,\eta)$ reduces to the (single) moment scaling exponent $K(q)$ for $\eta=1$. Fig. 5.9 gives some examples of various trace moments as a function of resolution; note that the scaling is very accurately followed. Without going into details, we just mention here the real advantage of the DTM-technique, which becomes apparent when it is applied to universal multifractals:

$$K(q, \eta) = \eta^\alpha K(q) \quad 5.5.3$$

α can therefore be estimated by the slope on a simple plot of $\log(K(q,\eta))$ vs. $\log \eta$ for fixed q . By varying q we improve the statistical accuracy. C_1 can be estimated as the intersection with the line $\eta=1$:

$$C_1 = K(q) \frac{\alpha-1}{q^\alpha - q} \quad 5.5.4$$

Finally, note that eq.5.5.2 is only valid when the relevant statistical moments converge (the critical value is q_D) and when the sample size is sufficiently large to accurately

estimate the scaling exponents (the critical value is q_s , corresponding to the maximum order of singularity γ_s present in the finite sample, see section 3.4b). Whenever $\max(q\eta, q) > \min(q_s, q_D)$ the above relation will break down; $K(q, \eta)$ will become independent of η .

Note a consequence of the direct relation 5.5.3: If φ is a conserved universal multifractal field, characterized by the indices $(\alpha_\varphi, C_{1(\varphi)})$, the field φ^a also is a universal multifractal field with the indices $(\alpha_{\varphi^a}, C_{1(\varphi^a)})$:

$$\alpha_{\varphi^a} = \alpha_\varphi = \alpha \quad 5.5.5a$$

$$C_{1(\varphi^a)} = a^\alpha C_{1(\varphi)} \quad 5.5.5b$$

This relation quantifies the assumption made at the beginning that $a=1$.

The DTM-Analysis was applied to the fractional differentiated data. The Double trace moments were calculated for 4 different values of q : $q=0.75, 1.5, 2.0, 2.5$. For all of these values the double trace moments show excellent scaling as shown in Figure 5.9 for $q=1.5$. The slopes of these graphs are equal to $(K(q, \eta))$. From the $\log(K(q, \eta))$ vs. $\log \eta$ (fixed q) graph (Figure 5.10) the universal multifractal indices can then be estimated. Notice the remarkable long and straight line part for the curves which breaks down for high values of η . In fact, the value of η for which the curves are bending towards the horizontal is consistent with the theoretical estimate $\eta \cong \frac{q_D}{q}$.

The following parameters were estimated from the slopes and intercepts of the straight parts:

q	α	C_1
0.75	1.98	0.061
1.50	1.99	0.063
2.00	1.99	0.063
2.50	1.99	0.063

Table 5.2: Estimated universal indices by the DTM-analysis technique.

The universal multifractal indices are: $\alpha = 1.99 \pm 0.01$ and $C_1 = 0.06 \pm 0.01$. This value of C_1 can be compared to the estimate obtained by the structure function in section 5.3: $C_1 \approx 0.09$. Both values are very small so that a minor discrepancy is to be expected. We averaged both values and obtained an overall estimate of $C_1 = 0.08 \pm 0.02$.

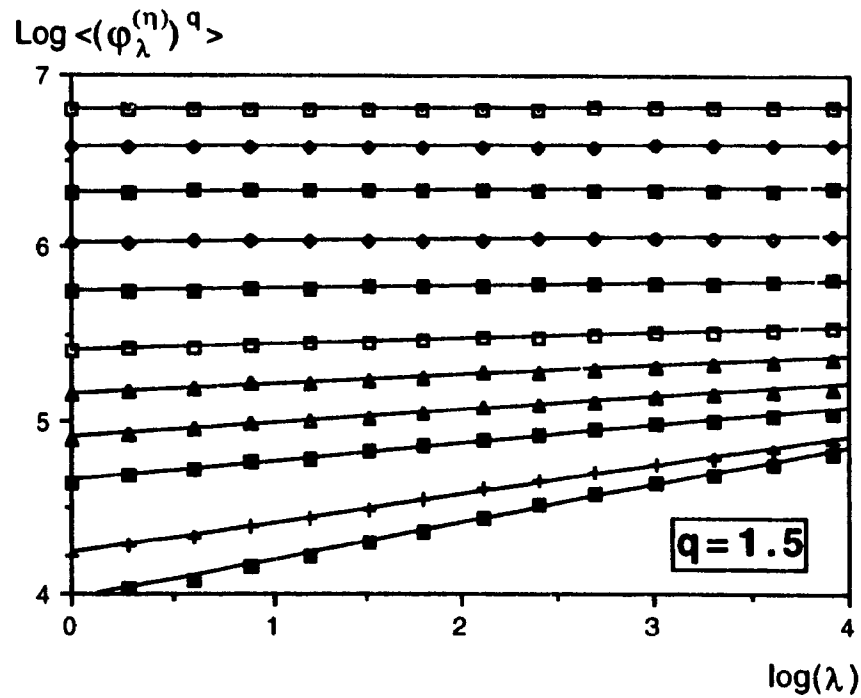


Figure 5.9: Scaling of the double trace moments $\log_{10}\langle(\varphi_\lambda^{(\eta)})^q\rangle$ versus $\log_{10}(\lambda)$. The lines correspond to a linear interpolation obtained with the values of η (from top to bottom): 0.10, 0.20, 0.32, 0.46, 0.62, 0.83, 1.00, 1.21, 1.47, 2.15, 3.16.

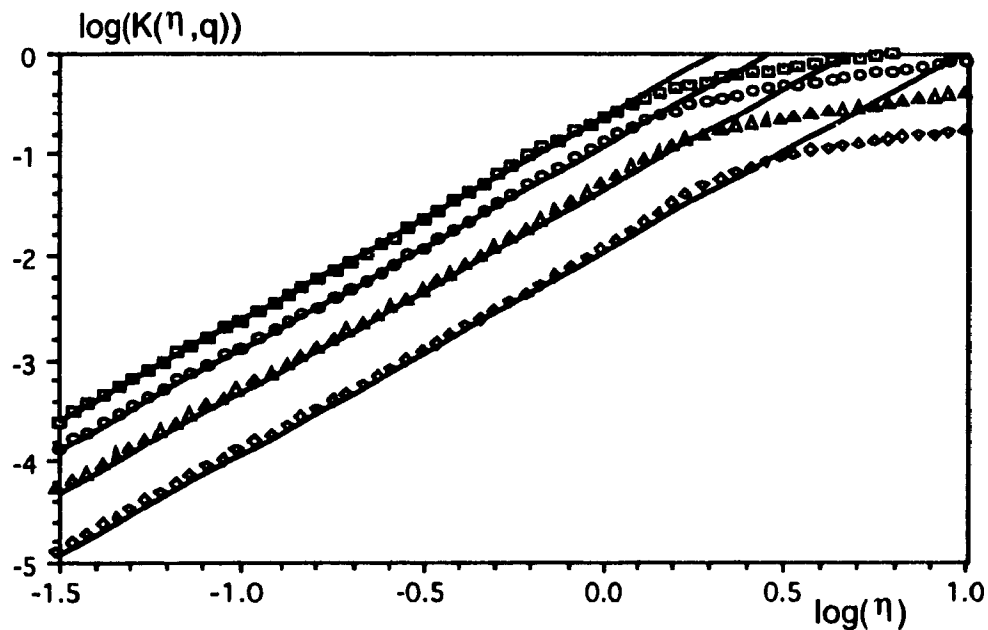


Figure 5.10: $K(q, \eta)$ as a function of η on \log_{10} - \log_{10} scale, for the values (top to bottom) $q=2.5, 2.0, 1.5, 0.75$. As expected for universal multifractals, the curves are linear and parallel for a certain range of the moments η . The parameter α can be identified as the slope of these straight line parts of the curves, whereas C_1 is the value of the straight line at the intersection $\eta=0$. For large values of η the slopes are bending towards the horizontal since $\max(q\eta, q) > \min(q_S, q_D)$.

5.6 Analysis of the statistical moments

The moment scaling exponent $K(q)$ (discussed in chapter 2 and 3) can be estimated directly by studying the scaling behavior of the dressed moments $\langle \phi_\lambda^q \rangle$ (see section 3.5). This is done by plotting $\log \langle \phi_\lambda^q \rangle$ versus $\log(\lambda)$ as shown in Figure 5.11. The straight lines indicate that the scaling is well respected: the slopes are the corresponding values of $K_d(q)$. Figure 5.12 shows the empirical $K_d(q)$ -function compared to the theoretical $K(q)$ -function obtained using $\alpha=2$ and $C_1=0.063$. There is an excellent agreement between the two curves in the range of $-0.5 < q < 2.5$. Note that the negative moments for the empirical $K_d(q)$ curve appear to be well behaved. This is an indicator, that the estimated data is lognormal ($\alpha=2$), since negative moments of q exist only for this type of universal multifractal.

For moments larger than the critical value $q \approx 2.3$, the empirical $K_d(q)$ curve becomes linear with a slope around 0.23 corresponding to a multifractal phase transition: it can be a second order phase transition due to sampling limitations (q_s), or a first order phase transition corresponding to divergence of the moments (q_D). The probability distribution of the absolute filtered field ϕ helps us to distinguish between these two qualitatively different multifractal phase transitions (Figure 5.13). The graph shows the probability distributions for different amounts of dressing (various λ 's). All distributions apparently have a hyperbolic tail,

$$\Pr(\phi > y) \propto y^{-q_D} \quad y \gg 1 \quad 5.6.1$$

where y is the absolute value of the filtered LWC-data. This corresponds to a linear behavior of the probability distribution exponent $c(\gamma)$ for orders of singularities γ beyond a critical value γ_D (see below) and divergence of moments with the critical value $q_D \approx 2.3$. Since $c(\gamma)$ is related to $K(q)$ via Legendre transformation we expect from the empirical $K(q)$ (Figure 5.12) $\gamma_D = K'(q)$ for $q > q_D$, i.e. $\gamma_D \approx 0.23$. In the next chapter we will see, that the empirical probability distribution exponent has indeed these features.

In section 5.3 where the structure function of the raw LWC-data was calculated, the critical value of q , at which the structure function $\zeta(q)$ became linear, was also at $q_D \approx 2.3$. The slope of the linear part was around 0.06. For values of $q > q_D$ this yields $K(q) = 0.23q$ (using the above estimate of $H \approx 0.29$ and equation 5.3.3). This value is in excellent agreement with the slope estimated directly from the empirical $K(q)$ function (Fig. 5.12) $\gamma_D \approx 0.23$ for $q > q_D$.

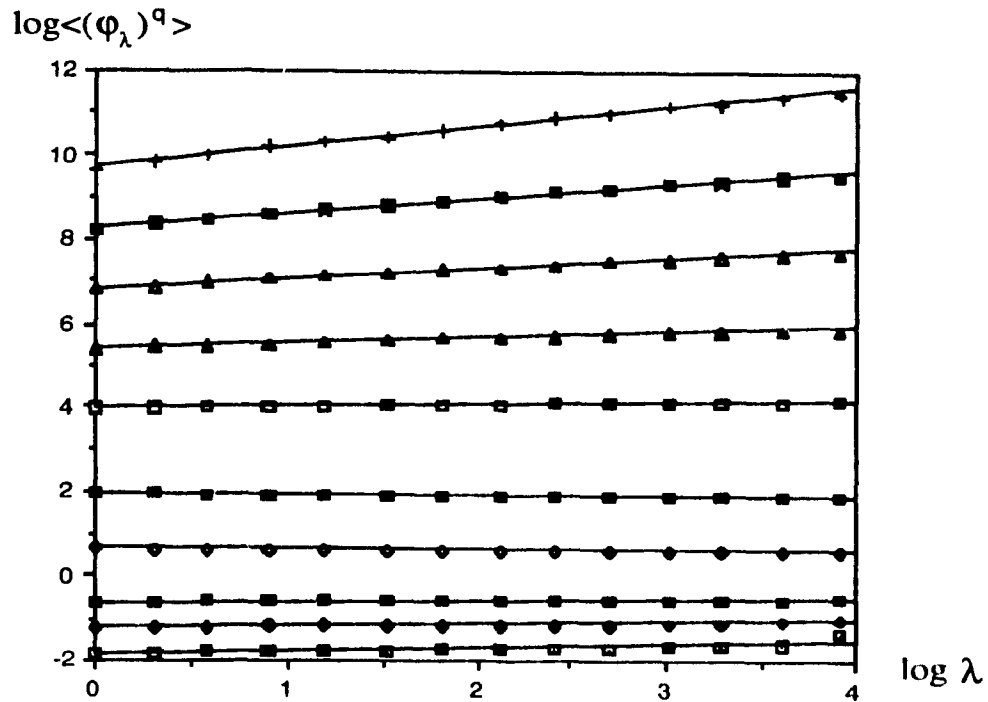


Figure 5.11: Scaling of the moments of the field φ , $\log_{10}\langle(\varphi_\lambda)^q\rangle$ versus $\log_{10}(\lambda)$. The lines correspond to a linear interpolation obtained with the values of q (from bottom to top): -0.75, -0.50, -0.25, 0.25, 0.75, 1.50, 2.00, 2.50, 3.00, 3.50.

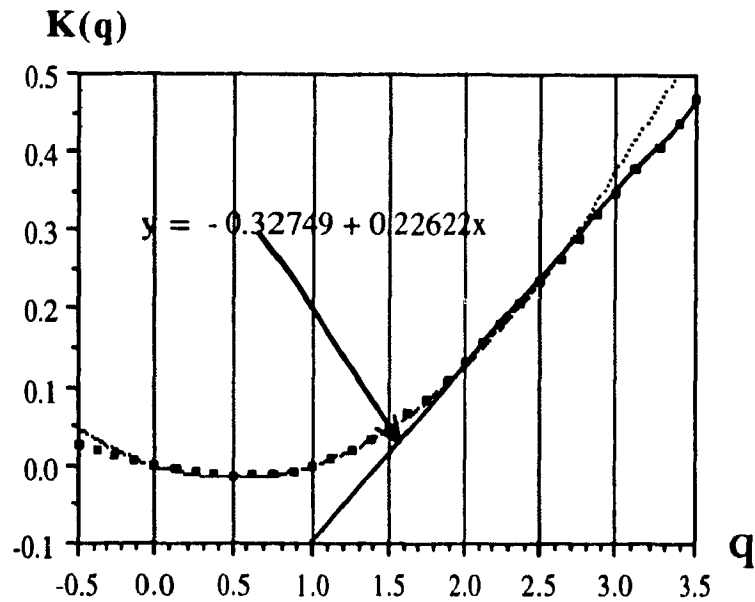


Figure 5.12 : Comparison of the empirical estimate of $K_d(q)$ with the lognormal universal multifractal $K(q)$ for $\alpha=2$ and $C_1=0.063$. There is an excellent agreement between the two curves for the moments with $-0.3 < q < 2.5$. Note that for the empirical $K_d(q)$ the negative moments are well behaved, which is an indicator that $\alpha=2$.

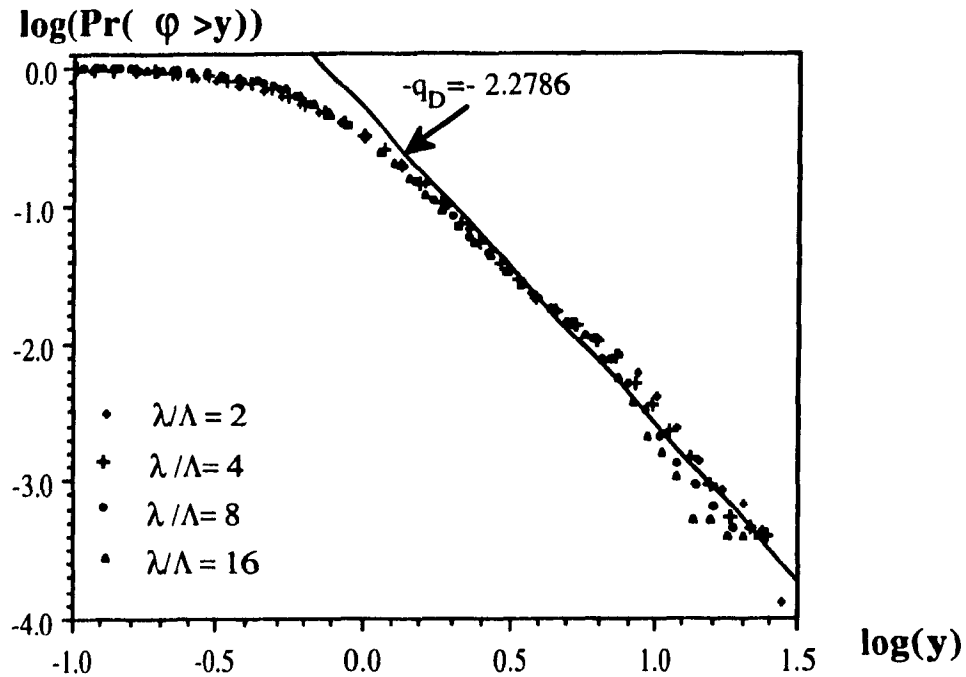


Figure 5.13: Probability-distribution $\log_{10}(\text{Pr}[\varphi > y])$ versus $\log_{10}[y]$ of the LWC-data, dressed by different amounts. $\lambda/\Lambda = 2, 4, 8, 16$. Note that the near superposition of the curves indicates the right amount of fractional differentiating of the data, which implies a fair estimate of $H=1/3$. Furthermore the distributions have a hyperbolic tail which is represented in the graph by the straight line whose absolute slope is the critical order of moment $q_D=2.3$.

5.7 Analysis of the probability distribution exponent

In order to confirm the universal multifractal indices estimated from the DTM in section 5.5, we analyze the absolute values φ of the power law filtered data with the PDMS technique (see section 3.3) and obtain the probability distribution exponent $c(\gamma)$. Remember that for each fixed order of singularity γ , the logarithm of the probability distribution is plotted versus the logarithm of the scale parameter λ (Figure 5.14). The scaling is most accurately followed over the range of $16 < \lambda < 2048$. For each order of singularity γ , linear regression in the scaling regime of λ yields an estimate of the empirical $c(\gamma)$. We compare this with the theoretical probability distribution exponent for a lognormal multifractal ($\alpha=2$) with $C_1=0.063$ (Figure 5.15). To obtain an overlap of both curves, the theoretical curve was shifted by 0.023 to the left which corresponds to a minor shift in γ . As expected, the estimated $c(\gamma)$ curve follows a straight line with the slope $c'(\gamma)=q_D \approx 2.3$ for orders of singularities larger than the critical $\gamma_D=K'(q_D) \approx 0.23$. Note the excellent agreement between the moment exponent behavior and the probability distribution exponent behavior beyond the critical values q_D, γ_D .

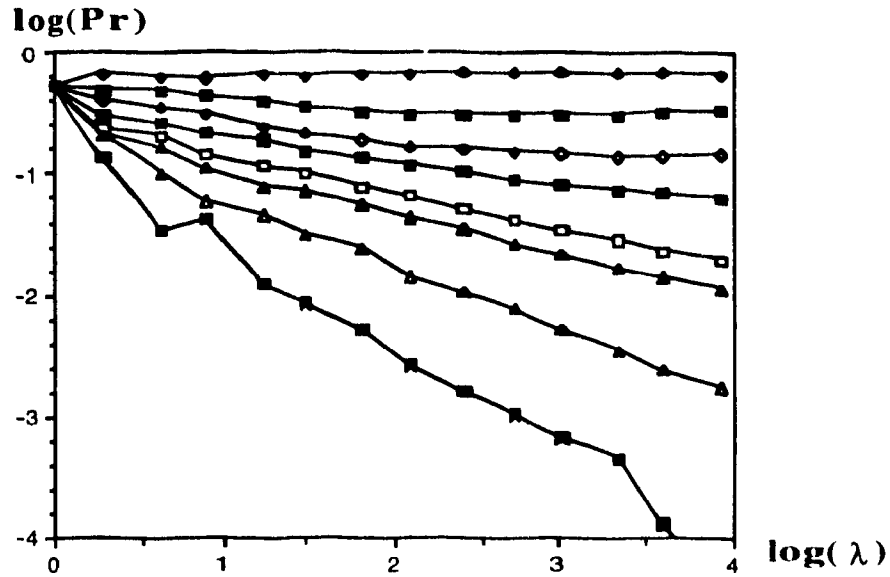


Figure 5.14: PDMS analysis of the absolute values of the power law filtered ($H=1/3$) LWC-data. The graph shows $\log_{10}(\text{Pr}[\varphi > \lambda^\gamma])$ versus $\log_{10}(\lambda)$ and its scaling in the range $16 < \lambda < 2048$. The lines are obtained for the following orders of singularities γ (from top to bottom): $-0.10, 0.00, 0.06, 0.10, 0.16, 0.20, 0.30, 0.40$.

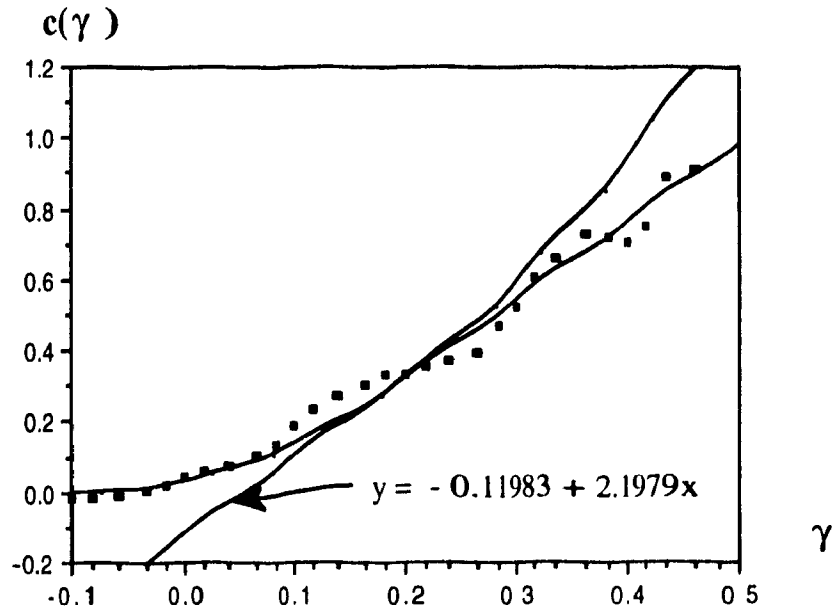


Figure 5.15: Comparison of the estimated probability distribution exponent with the theoretical $c(\gamma)$ -curve for $\alpha=2$ and $C_1=0.063$. The theoretical curve was shifted by a value $a=0.023$ to the left, to obtain a superposition of both curves. As expected, the estimated $c(\gamma)$ follows a straight line with the slope $c'(\gamma_D)=q_D=2.3$ for values of γ larger than the critical $\gamma_D \approx 0.23$, i.e. the tangent on the theoretical curve in the shifted graph at $\gamma \approx 2.1$.

5.8 Evidence for lognormal multifractal clouds

We now try to answer the question, in which we are most interested in: can our cloud-samples be described by lognormal universal multifractals ($\alpha=2$) or are they rather universal multifractals with an Levy index less than two ($\alpha=2-\epsilon$, ϵ small)? Although we can determine α with quite high precision (1.99 ± 0.01 , see table 5.2), it is important to know if it is exact equally two, since this qualitatively is a different class of universal multifractals than types where $\alpha < 2$. Lognormal multifractals are the only types of universal multifractals where the derivative of the probability distribution exponent becomes negative for small enough values of γ , corresponding to the existence of negative moments q . This implies that the regularities of the cloud (regions with very low density) become less probable the smaller the regularities (lower the density) become. Obviously, as already pointed out in previous chapters, the statistical behavior of the low density regions is very important in order to determine the radiative transfer properties (i.e. in these regions the photon free path length is very long, hence most of the transport occurs there). Furthermore the theoretical approach in section 2.5 needed a clearly defined minimum of the probability distribution exponent $c(\gamma)$ for the Laplace-method to work. Universal multifractals with $1 < \alpha < 2$ do not have a minimum since $c(\gamma)=0$ for all $\gamma < \gamma_{\min}$, where γ_{\min} is the largest value for which $c(\gamma)=0$.

In lognormal multifractals, the log-probability distribution is symmetric; $\Pr(\varphi > x) = \Pr(A/\varphi > x)$, with A a constant which depends here on λ and C_1 . This can be seen by considering the probability distribution exponent $c(\gamma)$ (eq. 2.2.6a): for lognormal multifractals this function is a parabola with the vertex at $\gamma = -C_1$, i.e. $-C_1$ is the symmetry point. All other types of universal multifractals with α less than two do not have such a symmetry in the probability distribution exponent.

In order to find out if at least in principle it is possible to see that difference with 15 realizations with 8192 data points each, we simulated fields of the same size as the empirical data with $C_1=0.063$ and $\alpha=1.99$, $\alpha=2.0$ respectively by means of the continuous cascade algorithm (section 3.1). The data was then rescaled (dressed) by a factor of 4, as we did with the empirical data to avoid possible oversampling problems with the empirical data at finest resolution. We plotted $\log(\Pr\{\varphi > y\})$ and $\log(\Pr\{1/\varphi > y\})$ versus $\log(y)$ on top of each other for both simulated fields (Figure 5.16). Note that on a log-log plot the latter probability distribution is the reflection of $\Pr\{\varphi < y\}$. The symmetry is clear to see in the lognormal multifractal case, however for $\alpha=1.99$ the distributions are not symmetric.

If we now make a similar plot with the empirical data, we find that both distributions appear to have the same hyperbolic tail and thus show nearly symmetric behavior (Figure 5.17). The existence of the symmetry indicates (assuming universality) that $1.99 < \alpha \leq 2$. This increases the confidence that the experimental cloud data can best be described by a lognormal multifractal. Figure 5.17 shows that also the probability distribution $\Pr[1/\varphi > y]$ has a hyperbolic tail, which means that we found negative temperature phase transitions.

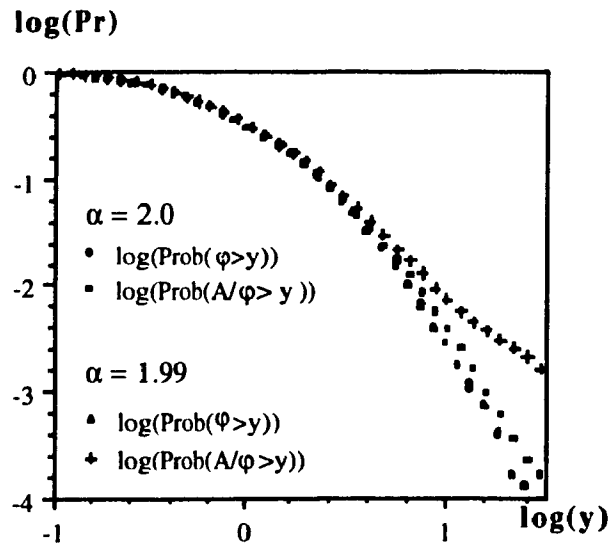


Figure 5.16: Probability distributions of a multifractal simulation (15 realization with 8192 data points each) with $\alpha=2.0$ and $\alpha=1.99$ (dressed by a factor 4). The graph compares both probability distributions: $\log_{10}(\text{Pr}(\varphi > y))$ and $\log_{10}(\text{Pr}(A/\varphi > y))$ versus $\log_{10}(y)$ for both fields. The constant A was chosen for the optimum superposition, $A=10^{0.45}=2.8$. Clear to see is the symmetry of both distributions in the lognormal multifractal case ($\alpha=2$). However for $\alpha=1.99$ both distributions are not symmetric.

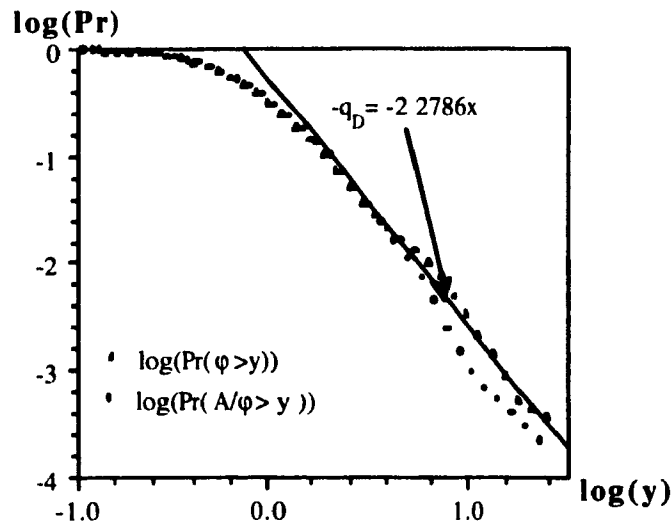


Figure 5.17: Probability-distribution of the LWC-data (dressed by a factor 4). The graph shows the symmetry of both probability distributions: $\log_{10}(\text{Pr}(\varphi > y))$ and $\log_{10}(\text{Pr}(A/\varphi > y))$ versus $\log_{10}(y)$. The constant A was chosen for the optimum superposition, $A=10^{0.3}=2$. The well respected symmetry of both curves indicates that $\alpha=2$. Furthermore the distributions have a hyperbolic tail which is represented in the graph by the straight line with the absolute slope the critical order of moment $q_D=2.3$. The hyperbolic tail for $(\text{Pr}(A/\varphi > y))$ corresponds to a negative temperature phase transition.

5.9 Conclusions of the empirical cloud data analysis

The "Singularity Formulation" of scattering as well as the "Renormalization" approach, introduced in chapter 2 and chapter 4 respectively, were developed for a lognormal multifractal cloud model. The analysis of stratocumulus cloud data performed in this chapter confirmed the applicability of lognormal multifractal clouds.

We analyzed empirical cloud liquid-water-content data in the spatial range between 5m to 330 km. The power spectra was scaling over the entire range, thus questioning the existence of the "mesoscale-gap". The spectral exponents were found close to the theoretical value in turbulence for passive scalars with $\beta_{\text{theo}}=5/3$, in fact we found a spectral slope of the ensemble averaged power spectrum $\beta=1.7$. This indicated that the LWC-field was not conserved and $H \approx 1/3$. A study of the structure function $\zeta(q)$ yielded $C_1 \approx 0.09$ and $H \approx 0.29$, the latter being close to the passive scalar value in standard turbulence. These values of C_1 and H are very close to those found by Davis et al 1994 using only a single sample. The structure function also suggested there was a multifractal phase transition with critical exponent $q_D \approx 2.3$.

We fractionally differentiated (power law filtered) the fields by λ^H , retrieving a conserved field which was then analyzed. A Double-Trace-Moment (DTM) was applied to directly estimate the universal multifractal indices and yielded $\alpha = 1.99 \pm 0.01$ and $C_1 = 0.06 \pm 0.01$. A comparison of the empirical moment scaling function with the theoretical $K(q)$ -function showed consistency with the DTM estimates up to a critical exponent $q_D \approx 2.3$. In order to determine the nature of this phase transition we examined the probability distribution function. A log-log plot indicated a hyperbolic tail corresponding to divergence of moments with a slope $q_D \approx 2.3$. Furthermore a Probability Distribution/Multiple Scaling (PDMS) analysis yielded the empirical $c(\gamma)$ -function and confirmed the estimated multifractal indices with a first order phase transition occurring at $\gamma_D \approx 0.23$.

Since it is of profound interest for the radiative properties of the cloud if it can be described by a lognormal multifractal, we showed that the logs of the probability distribution functions $\Pr(\phi > y)$ and $\Pr(1/\phi > y)$ are nearly equal, thus giving strong evidence for a lognormal multifractal cloud. Since the asymptotic tail of $\Pr(1/\phi > y) \approx y^{-q_D}$ this indicates the existence of a negative temperature phase transition for $q < q_D$

Summarizing, the following multifractal indices were found: $\alpha \approx 2$; $C_1 = 0.08 \pm 0.02$; $H \approx 0.29$ and a second order phase transition at $q_D \approx 2.3$.

6. Conclusions

In recent years it has been shown that a realistic study of the Earth's climate system, e.g. by general circulation models (GCM's), needs improved modeling of clouds to take into account their strong inhomogeneity as well as to better understand their related radiative properties. Most numerical modeling of the radiation effect of clouds has assumed a plane-parallel geometry despite the considerable three dimensional variability, in the density field, geometry and spacing. The purpose of this work is to justify the use of multifractals as highly inhomogeneous models for clouds and to provide a formalism retrieving radiative transfer properties in these media.

We analyzed stratocumulus cloud liquid water content data from the 1987 FIRE experiment. The data showed excellent scaling over the entire spatial range of 5m-330km. The universal multifractal indices were estimated with the results: $\alpha \approx 2$, $C_1 = 0.08 \pm 0.02$ and $H \approx 0.29$. With several methods we demonstrated that the examined cloud data responded like a lognormal multifractal with $\alpha = 2$, thus providing a motivation for studying radiative transfer in universal lognormal multifractals.

In the main part of this work, we developed a formalism analogous to the multifractal singularity formalism for understanding photon scattering statistics in radiative transfer in multifractals with existing negative moments $q = c'(\gamma) < 0$. Using the nondimensional extinction coefficient κ to characterize the optical thickness and the transport properties proved to be a tractable approach to calculate the "bare" photon statistics. The theory involved two fundamental quantities: (1) The moment scaling exponent $K_p(q)$ which characterizes the scaling of the moments of the free photon path distribution, and could be exactly calculated in the case of a lognormal multifractal medium. (2) The probability distribution exponent $c_p(\gamma_p)$ that determines the scattering probabilities for photon path distances. It was approximated in two different ways, leading to the same result. We performed extensive numerical tests of the results and consequently obtained the dressed statistics. We showed that the "bare" and the "dressed" statistics are not significantly different and so justified our theoretical "bare" approach. Although the results are only exactly valid in the thick cloud (large extinction coefficient κ) limit, the approximation was found to be quite accurate down to $\kappa \approx 1-10$, so that the results may be widely applicable.

It was shown that the near linearity of $K_p(q)$ led to the possibility of "renormalizing" the multifractal by replacing it with a near equivalent homogeneous medium but with an effective extinction coefficient $\kappa^{1/(1+C_1)}$ where C_1 is the codimension

of the mean singularity of the cloud. The "renormalizing" approach provides an easy tool to estimate the bulk radiative properties of a lognormal multifractal cloud. Finally, we argued that this approximation was likely to continue to be valid for multiple scattering, and was also compatible with recent results for diffusion on lognormal multifractals. We compared our results with recent numerical calculations finding excellent agreement.

One limitation of these results was their restriction to the rather special lognormal case ($\alpha=2$). The key point in the above development is the approximation of the bare multifractal properties by the dressed ones. When $\alpha < 2$, this step is still straightforward for the larger singularities, but may breakdown for the regularities associated with the numerous weak "Levy hole" events that will dominate the scattering. However, preliminary numerics indicate that even here, similar treatment may be possible using appropriate asymptotic dressed multifractal properties. This is an important area for future work.

Appendix

A1 Evaluation of the Moment Scaling Exponent

The transmission is calculated as (2.5.6)

$$\langle T(x) \rangle = \sqrt{\frac{\log \kappa}{4C_1 \pi (1 - \gamma_p)}} \int_{-\infty}^{\infty} e^{\frac{-\log \kappa}{4C_1(1-\gamma_p)} [(1-\gamma_\tau) - (1+C_1)(1-\gamma_p)]^2} e^{-\kappa \gamma_\tau} d\gamma_\tau \quad \text{A1.1}$$

In order to calculate the moment scaling exponent $K_p(q)$ (eq. 2.5.3) exactly we use the fact that $\langle T \rangle = \Pr(\tau_p > \kappa x)$ and so the probability density for γ_p is

$$p(\gamma_p) d\gamma_p = -\frac{\partial \langle T \rangle}{\partial \gamma_p} d\gamma_p. \quad \text{A1.2}$$

The moments of τ_p can now be found from

$$\langle \tau_p^q \rangle = -\int_{-\infty}^1 \frac{\partial \langle T \rangle}{\partial \gamma_p} \kappa^{q\gamma_p} d\gamma_p. \quad \text{A1.3}$$

The integral can be done exactly. Integrating by parts gives

$$\langle \tau_p^q \rangle = -\kappa^q e^{-\kappa} + q \log \kappa \int_{-\infty}^1 \langle T \rangle \kappa^{q\gamma_p} d\gamma_p, \quad \text{A1.4}$$

where we have used the fact that $\langle T(\gamma_p = 1) \rangle = \langle T(x = 1) \rangle = e^{-\kappa}$. The trick now is to reverse the order of integration and integrate over γ_p first. Using the definitions $\beta = 1 + C_1$ the integral in eq. A1.4 can be written

$$I_1 = \int_{-\infty}^1 \langle T \rangle \kappa^{q\gamma_p} d\gamma_p = \sqrt{\frac{\log \kappa}{4\pi C_1}} \int_{-\infty}^{\infty} e^{-\kappa \gamma_\tau} I_2(\gamma_\tau) d\gamma_\tau, \quad \text{A1.5}$$

where

$$I_2(\gamma_\tau) = \int_{-\infty}^1 e^{-\log \kappa \frac{[\sigma - \beta(1-\gamma_p)]^2}{4C_1(1-\gamma_p)}} \kappa^{q\gamma_p} \frac{d\gamma_p}{\sqrt{1-\gamma_p}}. \quad \text{A1.6}$$

Using $\int_0^{\infty} x^{-1/2} e^{-(ax+b/x)} dx = \sqrt{\frac{\pi}{a}} e^{-2\sqrt{ab}}$, we obtain

$$I_2(\gamma_\tau) = \sqrt{\frac{4C_1\pi}{\log \kappa (\beta^2 + 4C_1q)}} \kappa^{q - \frac{\sigma}{2C_1}(\sqrt{\beta^2 + 4C_1q} - \beta)} \quad \text{A1.7}$$

With the shorthand $s = \frac{1}{2C_1}(\sqrt{\beta^2 + 4C_1q} - \beta)$,

$$I_1 = \sqrt{\frac{1}{\beta^2 + 4C_1q}} \kappa^{q-s} \int_{-\infty}^{\infty} \exp(-\kappa^{\gamma_\tau} + s \gamma_\tau \log \kappa) d\gamma_\tau = \sqrt{\frac{1}{\beta^2 + 4C_1q}} \kappa^{q-s} \frac{\Gamma(s)}{\log \kappa} \quad \text{A1.8}$$

Putting everything together:

$$\langle \tau_p^q \rangle = -\kappa^q e^{-\kappa} + \sqrt{\frac{1}{\beta^2 + 4C_1q}} q \Gamma(s) \kappa^{q-s} \quad \text{A1.9}$$

$$\langle \tau_p^q \rangle = -\kappa^q e^{-\kappa} + f(q) \kappa^{q-s} \quad \text{A1.10}$$

We conclude that except for the leading term which becomes small exponentially fast with κ (and which arose because the external scale of the cloud is 1) the moment function is scaling in κ . If we write

$$\langle \tau_p^q \rangle \sim \kappa^{K_p(q)}, \quad \text{A1.11}$$

then

$$K_p(q) = q - \frac{1}{2C_1}(\sqrt{\beta^2 + 4C_1q} - \beta) \quad \text{A1.12}$$

A2 Laplace Method for the Evaluation of the Probability Distribution Exponent

The transmission is calculated as (2.5.6). We can write that integral with κ as the base:

$$\langle T(x) \rangle = \sqrt{\frac{\log \kappa}{4C_1\pi(1-\gamma_p)}} \int_{-\infty}^{\infty} \kappa^{-\frac{1}{4C_1(1-\gamma_p)}[(1-\gamma_r)-(1+C_1)(1-\gamma_p)]^2} \kappa^{-\frac{\kappa^{\gamma_r}}{\log \kappa}} d\gamma_r \quad \text{A2.1}$$

The Laplace method consists in evaluating the integral at the minimum of the exponent. In the limit of large κ this yields:

$$c_p(\gamma_p) = \min_{\gamma_r} \left(\frac{[(1-\gamma_r)-(1+C_1)(1-\gamma_p)]^2}{4C_1(1-\gamma_p)} + \frac{\kappa^{\gamma_r}}{\log \kappa} \right). \quad \text{A2.2}$$

The minimum occurs for $\gamma_r \approx 0$ which leads to eq. 2.5.9. Note that the extent to which the prefactor $f(q)$ (eq. A1.10) affects the scaling shows up in the second order correction to γ_r .

Bibliography

- Albrecht, B. A., D. A. Randall, and S. Nicholls, 1988, "Observations of Marine Stratocumulus Clouds During FIRE", *Bull. Am. Meteor. Soc.*, **69**, 618-626.
- Atmanspacher, H., H. Scheingraber, and G. Weidenmann, 1989, "Determination of $f(\alpha)$ for a limited random point set", *Phys. Rev. A*, **40**, pp. 3954.
- Barker H. W. and J. A. Davies, 1992, "Solar Radiative Fluxes for Stochastic, Scale-invariant Broken Cloud Fields", *J. Atmos. Sciences*, **49**, 1115-1126.
- Benzi, R., G. Paladin, G. Parisi, and A. Vulpiani, 1984, "On the multifractal nature of fully developed turbulence", *J. Phys.. A.*, **17**, 3521-3531.
- Cahalan, R. F., 1989, "Overview of Fractal Clouds", paper presented at RSRM'87, *Advances in Remote Sensing*, 371-389, edited by A. Deepak et al., A. Deepak, Hampton, Va.
- Cahalan, R. F., 1994, "Bounded cascade clouds: albedo and effective thickness", *Nonlinear processes in Geophysics*, in press.
- Chandrasekhar, S., 1946, *Astrophys. J.*, **105**, pp. 351; **104**, pp.110.
- Chandrasekhar, S., 1960, "Radiative Transfer", *Dover Publications, Inc.*, New York .
- Corrsin, S., 1951, "On the spectrum of isotropic temperature fluctuations in an isotropic turbulence", *J. Appl. Phys.*, **22**, 469-473.
- Davies, R., 1984, "Reflected solar radiance from broken cloud scenes and the interpretation of scanner measurements, *J. Geophys. Res.*, **89**, 1259-1266.
- Davis, A., P. Gabriel, S. Lovejoy, D. Schertzer, 1988, "Scaling Laws For Asymptotically Thick Clouds, Dimensional Dependence - Phase Function Independence", *IRS proceedings*, 103-106.
- Davis, A., P. Gabriel, S. Lovejoy, D. Schertzer, G. L. Austin, 1990, " Numerical Results And Meteorological Applications", *Geophys. Res.*, **95**, 11729-11742.
- Davis, A., S. Lovejoy, D. Schertzer, 1991, "Discrete angle radiative transfer in a multifractal medium", *SPIE-Proceedings*, vol. 1558, 37-59.
- Davis, A., S. Lovejoy, D. Schertzer, 1993, "Supercomputer Simulation Of Radiative Transfer In Multifractal Cloud Models", *IRS-Proceedings*, 112-115.
- Davis, A., 1992, "Radiation Transport in Scale Invariant Optical Media", Ph.D. thesis, McGill University, Montréal, Québec, Canada.
- Davis, A., A. Marshak, and W. Wiscombe, 1994, "Wavelet-Based multifractal Analysis Of Non-Stationary And/OR Intermittent Geophysical Signals", submitted to *"Wavelet Transforms in Geophysics"*.
- Evans, K. F., 1993, "A General Solution For Stochastic Radiative Transfer", *G.R.L.*, **20**, 19, 2075-2078.
- Francis F., T. Falco, S. Lovejoy, D. Schertzer, B. Kerman, M. Drinkwater, and C. Livingston, 1994, "Scale invariance and universal multifractals in sea ice synthetic aperture radar reflectivity fields, submitted to *J. Geophys. Res.*.
- Frisch, U., P. L. Sulem, and M. Nelkin, 1989, "A simple dynamical model of intermittency in fully developed turbulence", *J. Fluid Mech.*, **87**, 719-724.
- Gabriel, P., S. Lovejoy, G.L. Austin, and D. Schertzer, 1986, "Radiative transfer in extremely variable fractal clouds", paper presented at the *6th Conference on Atmospheric Radiation*, Am. Meteorol. Soc., Williamsburg, Va., May 12-16.

- Gabriel, P., S. Lovejoy, D. Schertzer, and G.L. Austin, 1988, "Multifractal analysis of resolution dependence in satellite imagery", *Geophys. res. Lett.*, **15**, 1373-1376.
- Gabriel, P., S. Lovejoy, A. Davies, D. Schertzer, G. L. Austin, 1990, "Renormalization Approach For Homogeneous And Fractal Clouds", *Geophys. Res.*, **95**, 11717-11728.
- King, W. D., C. T. Maher, and G. A. Hepburn, 1981, "Further performance tests on the CSIRO liquid water probe", *J. Appl. Meteor.*, **20**, 195-202.
- Kolmogorov, A. N., 1941, "Local Structure of Turbulence in an Incompressible Liquid for Very Large Reynolds Numbers", *Dokl. Akad. Sci. USSR*, **30**, 299-303.
- Kolmogorov, A. N., 1962, "A refinement of previous hypothesis concerning the local structure of turbulence in viscous incompressible fluid at high Reynolds number", *J. Fluid Mech.*, **83**, pp. 349.
- Korvin, G., 1992, "Fractal models in earth Sciences", *Elsevier*, pp.396.
- Ladoy, P., F. Schmitt, D. Schertzer et S. Lovejoy, 1993, "Variabilité temporelle multifractale des observations pluviométriques a Nimes", *C. R. Acad. Sci. Paris*, **317**, II, 775-782.
- Lam, N. S.-N., L. de Cola, 1993, "Fractals in Geography", *PTR Prentice Hall*.
- Lavallée, D., 1991, "Multifractal techniques: Analysis and simulation of turbulent fields", Ph.D. thesis, McGill University, Montréal, Québec, Canada.
- Lavallée, D., S. Lovejoy, and D. Schertzer, 1991a, "On the determination of the codimension function", in *Non-linear variability in geophysics: Scaling and fractals*, Kluwer, Schertzer, D. and S. Lovejoy, 99-110.
- Lavallée, D., S. Lovejoy, D. Schertzer, and P. Ladoy, 1993, "Nonlinear variability, multifractal analysis and simulation of landscape topography, in: DeCola, L., and N. Lam (Editors), *Fractals in Geography*.
- Lovejoy, S., D. Schertzer, and A.A. Tsonis, 1987, "Functional Box-Counting and Multiple Dimension in rain, *Science*, **225**, 1036-1038.
- Lovejoy, S., P. Gabriel, D. Schertzer, and G.L. Austin, 1988, "Fractal Clouds With Discrete Angle Radiative Transfer", *IRS proceedings*, 99-102.
- Lovejoy, S., A. Davis, P. Gabriel, D. Schertzer, G. L. Austin, 1990, "Discrete Angle Radiative Transfer - Part I: Scaling and Similarity, Universality and Diffusion", *Geophys. Res.*, **95**, 11699-11715.
- Lovejoy, S., D. Schertzer, and B. Watson, 1993, "Radiative Transfer and Multifractal Clouds: theory and applications", in *I.R.S. 92*, A. Arkin, pp., in press.
- Mandelbrot, B. B., 1974, "Intermittent turbulence in self-similar cascades: divergence of high moments and dimension of the carrier", *J. Fluid Mech.*, **62**, 331-350.
- Marshak, A., W. Wiscombe, A. Davis, 1993, "On The Analysis Of The Multifractal Properties Of Cloud Liquid Water Data", *IRS 92 Proceedings*, A. Deepak, 116-119.
- Meneveau, C. and K. R. Sreenevasan, 1987, "Simple multifractal cascade model for fully developed turbulence", *Phys. Rev. Lett.*, **59**, 1424-1427.
- Monin, A. S., 1972, "Weather Forecasting as a Problem in Physics", *MIT Press*.
- Novikov, E. A. and Stewart, 1964, "Intermittency of turbulence and spectrum of fluctuations in energy-dissipation", *Izv. Akad. Nauk. SSSR. Ser. Geofiz*, **3**, 408-412.

- Obhukhov, A., 1949, "Structure of the temperature field in a turbulent flow", *Izv. Akad. Nauk. SSSR. Ser. Geogr. i Geofiz.*, **13**, 55-69.
- Obhukhov, A., 1962, "Some specific features of atmospheric turbulence", *J. Geophys. Res.*, **67**, pp. 3011.
- Paladin, G. and A. Vulpiani, 1987, "Anomalous scaling laws in multifractal objects", *Phys. reports*, **156**, 147-225.
- Parisi, G., and U. Frisch, 1985, "A multifractal model of intermittency", in *turbulence and predictability in geophysical fluid dynamics*, North Holland, Ghil, M., R. Benzi, and G. Parisi, 111-144.
- Preisendorfer, R.W., and G.L. Stephens, 1984, "Multimode radiative transfer in finite optical media", 1, Fundamentals", *J. Atmos. Sci.*, **41**, 709-724.
- Ramanathan, V., E.J. Pitcher, R. C. Malone, and M.L. Blackmon, 1983, "The response of a spectral general circulation model to refinement in radiative processes", *J. Atmos. Sci.*, **40**, 605-630.
- Ramanathan, V., E.J. Pitcher, R. C. Malone, and M.L. Blackmon, 1989, "Cloud-radiative forcing and climate: Results from the Earth Radiation Budget Experiment", *Science*, **243**, 57-63.
- Randall, D. A., J. A. Coakley, Jr., C. W. Fairall, R. A. Kropfli, and D. H. Lenschow, 1984, "Outlook for research on subtropical marine stratiform clouds", *Bull. Amer. Meteor. Soc.*, **65**, 1290-1301.
- Ronholm, K., M.B. Baker, and H. Harrison, 1980, "Radiative transfer through media with uncertain or variable parameters", *J. Atmos. Sci.*, **37**, 1279-1290.
- Salvadori, G., S.P. Ratti, G. Belli, S. Lovejoy, and D. Schertzer, 1993, "Multifractal Objective Analysis of Seveso Ground Pollution, *Toxicological and Environmental Chemistry*, in press.
- Schertzer D., and S. Lovejoy, 1983, "Elliptical turbulence in the atmosphere", in *proceedings of the fourth symposium on turbulent shear flows 11.1-11.8*, Karlsruhe, West Germany.
- Schertzer, D. and S. Lovejoy, 1987a, "Singularités anisotrope, divergence des moments en turbulence", *Ann. Sc. math. du Québec*, **11**, 1, 139-181.
- Schertzer, D. and S. Lovejoy, 1987b, "Physical modeling and Analysis of Rain and Clouds by Anisotropic Scaling of Multiplicative Processes", *J. Geophys. Res.*, **92**, 8, 9693-9714.
- Schertzer, D. and S. Lovejoy, 1989, "Nonlinear variability in geophysics: multifractal analysis and simulation", in *Fractals; Physical Origin and Consequences*, Plenum, Pietronero, L. , New York, 49-79.
- Schertzer, D. and S. Lovejoy, 1991, "Nonlinear geodynamical variability: multiple singularities, universality and observables". In *non-linear variability in Geophysics; scaling and fractals*. Kluwer, Schertzer, D., and Lovejoy S., 41-82.
- Schertzer, D., S. Lovejoy, and D. Lavallée, 1993, "Generic multifractal phase transitions and self-organized criticality", in *Cellular Automata: prospects in astronomy and astrophysics*, World Scientific, Perdag, J. M. and A. Lejeune, 216-227.
- Schmitt, F., D. Lavallée, S. Lovejoy, D. Schertzer and C. Hooge, 1992, "Estimations directes des indices de multifractals universels dans le champ de vent et de temperature", *C. R. Acad. Sci. Paris*, **314 serie II**, pp. 749.

- Schmitt, F., 1993, "Fully developed turbulence and universal multifractals in wind tunnel and the atmosphere", PhD thesis, Pierre and Marie Curie University, Paris.
- Scholz C. H., and B. B. Mandelbrot, 1989, "Fractals in geophysics", *Birkhäuser*.
- Schuster, A., 1905, *Astrophys. J.*, **21**, 1.
- Silas, P., 1994, M.Sc. Thesis, McGill University, Montréal (Québec), Canada.
- Stephens, G.L., and R.W. Preisendorfer, " Multimode radiative transfer in finite optical media", II, Solutions, *J. Atmos. Sci.*, **41**, 725-735.
- Tessier, Y., S. Lovejoy, and D. Schertzer, 1993a, "Universal Multifractals: Theory and Observations for Rain and Clouds", *J. Appl. Meteorology*, **32**, 223-250.
- Tessier, Y., S. Lovejoy, D. Lavallée, D. Schertzer and B. Kerman, 1993b, "Universal multifractal indices for the ocean surface at far red wavelengths", *Geophys. Res. Lett.*, **20**, 1167-1170.
- Titov, G. A., 1980, "Statistical characteristics of short wavelength solar radiation in the presence of cumulus cloudiness", *Izv. Acad. Sci. USSR Atmos. Oceanic Phys.*, **16**, 500-505.
- Welch, R.M., and W.G. Zdunkowski, 1981, "The radiative characteristics of noninteracting cloud fields", II, Calculations for cloud fields, *Contrib. Atmos. Phys.*, **54**, 273-285.
- Wendling, P., 1977, "Albedo and reflected radiance of horizontally inhomogeneous clouds, *J. Atmos. Sci.*, **34**, 642-650.
- Yaglom, A. M., 1966, "The influence on the fluctuation in energy dissipation on the shape of turbulent characteristics in the inertial interval", *Sov. Phys. Dokl.*, **2**, 26-30.